NASA TECHNICAL REPORT

NASA TR R-189

NASA TR R-189

PULSE-FREQUENCY-MODULATION TELEMETRY

by Robert W. Rochelle

Goddard Space Flight Center
Greenbelt, Maryland

NATIONAL AERONAUTICS AND SPACE ADMINISTRATION • WASHINGTON, D. C. • JANUARY 1964

PULSE-FREQUENCY-MODULATION TELEMETRY

By Robert W. Rochelle

Goddard Space Flight Center
Greenbelt, Maryland

NATIONAL AERONAUTICS AND SPACE ADMINISTRATION

For sale by the Office of Technical Services, Department of Commerce,
Washington, D.C. 20230 -- Price $1.50

PULSE-FREQUENCY-MODULATION TELEMETRY

by
Robert W. Rochelle
Goddard Space Flight Center

SUMMARY

This report is concerned with the heuristic development of the basic features of pulse-frequency modulation, an information encoding technique which has been used in a number of spacecraft. The primary advantages are its noise-immunity characteristics and its ease of generation. A description of the present method of formating and synchronization is presented in order to illustrate the convenient handling of both analog and digital data.

The theory of group-coded binary sequences is derived by using a special type of correlation matrix. By combining particular sequences from a number of these correlation matrices, a new matrix is generated which is identical to the correlation matrix of a set of pulse-frequency modulation words. Thus, it is shown that pulse-frequency modulation has the same communication efficiency as a comparable set of coded binary sequences with an equal number of quantized levels.

In the detection process for PFM signals, a set of contiguous unmatched filters is used to enhance the signal-to-noise ratio. To examine the effects of Rayleigh noise on the output of these filters, the word-error probability is derived as a function of the energy per bit, noise power density, and degree of coding. The same development is given for the matched-filter case.

The analysis of the excitation of an unmatched filter to a step sinusoid is carried out to indicate the magnitude of the errors affecting the direct frequency measurement of the pulsed sine wave. The analysis also covers the action of a pulsed sine wave in which the frequency is changing as it passes through the filter.

Experimental results from the spectral analyses of satellite recordings perturbed with random noise are presented to illustrate the noise-immunity characteristic of pulse-frequency modulation.

CONTENTS

Summary i

INTRODUCTION 1

The Encoding Problem 1
History of Coded Telemetry 2

CHARACTERISTICS OF PULSE-FREQUENCY MODULATION 3

General Description 3
Design Considerations 4

CHARACTERISTICS OF CODED BINARY SEQUENCES . . . 7

Group Coding 7
Parity Codes 10
PFM Correlation Table 11

NOISE ANALYSIS 13

Unmatched Filter 14
Matched Filter 22

CONTIGUOUS-FILTER DETECTION SYSTEM 28

Analysis of Unmatched Filters 30
Matched-Filter Techniques 32

EXPERIMENTAL RESULTS 34

Spectral Analysis 34
Signal-to-Noise-Ratio Comparisons 38

CONCLUSION 41

ACKNOWLEDGMENTS 43

References 43

Appendix A—Amplitude Density Spectrum of a Pulsed Sine Wave 45

Appendix B—Autocorrelation Function for Gaussian Noise . 47

Appendix C—Response of a Single-Pole Filter to a Step Sinusoid 49

Appendix D—Response of a Single-Pole Filter to a Changing Frequency 53

PULSE-FREQUENCY-MODULATION TELEMETRY*

by
Robert W. Rochelle
Goddard Space Flight Center

INTRODUCTION

The problem of communicating over large distances with minimum power is particularly challenging in view of the advances in information theory during the last 2 decades. With this theory as a guide, a number of interesting types of communication systems can be postulated which, in the limit, approach the theoretical maximum communication efficiency. The encoding methods of some of these systems are exceedingly complex in their implementation. The ideal type of system retains a high communication efficiency with little loss in simplicity. Pulse-frequency modulation is an attempt to fulfill these two basic criteria.

Pulse-frequency modulation (PFM) has been successfully employed as the information encoding technique in a number of small (< 200 lb) scientific satellites and space probes where the reduction of spacecraft power and weight was a prime consideration. The use of such systems leaves a greater percentage of the spacecraft available for scientific instrumentation. Since little information has appeared in the literature on the subject, it is hoped that this work will provide a background for practical usage, as well as a theoretical derivation, of pulse-frequency modulation.

The Encoding Problem

Telemetry implies measurement at a distance. The concept of modern telemetry includes the gathering and encoding of information at a remote station, transmitting this encoded signal to the receiving station, decoding the signal at this station, and presenting the measurements in an acceptable form. The transmission path may involve propagation by radio, light, or even sound waves. Attenuation of the transmitted signal is usually a predominant factor because of the physical separation between the transmitting and receiving apparatus. If attenuation is low, the choices of the encoding and modulation methods are not critical, and methods which lead to simple and reliable systems are usually employed. With the introduction of attenuation in the transmission path, interference in various forms may perturb the signals and cause transmission errors. By proper encoding of the information, the effect of these noise perturbations can be minimized. The amount of

*This report was submitted to the University of Maryland as partial fulfillment of the requirements for the degree of Doctor of Philosophy.

improvement or immunization to noise that can be accomplished is governed by Shannon's channel capacity theorem (Reference 1):

$$C = B \log_2 \frac{P + N}{N} , \quad (1)$$

where C is the channel capacity (bits per second), B is the channel bandwidth, P is the signal power, and N is the average noise power. As the signal power is decreased, the bandwidth of the encoded signal must be increased to maintain the same channel capacity and probability of error.

Various schemes can be devised to take advantage of Shannon's channel capacity theorem and thereby reduce the transmitter power for a given information rate. Kotel'nikov has described the general theory of high efficiency encoding (Reference 2). The problem involved is to approach the Shannon channel-capacity limit as closely as possible. But this must be consistent with the ability to implement the encoding scheme with equipment which is not of undue complexity. A practical example of this problem is the telemetering of scientific data from satellites and space probes. Since spacecraft power is limited, savings in transmitter power due to efficient coding can extend either the range or information rate or both. The improvement is greater in the small satellite class (< 200 lb), where a larger percentage of the satellite weight is devoted to the transmitter power system.

History of Coded Telemetry

Coded telemetry began with the early work on frequency modulation. At that time frequency modulation was thought to require less bandwidth than amplitude modulation, since the frequency deviation could be made smaller than the modulating frequency. Carson disproved this theory in 1922 (Reference 3). In 1936 Armstrong demonstrated the major advantage of frequency modulation–the improvement of the signal-to-noise ratio for large frequency deviations (Reference 4). The system traded bandwidth for signal-to-noise-ratio improvement. A recognized deficiency was the sharp threshold or decrease in the signal-to-noise ratio at low signal levels.

Pulse-code modulation* developed much more slowly than frequency modulation (Reference 5). It was not until 1948 that Shannon predicted that pulse-code modulation would have error-reducing properties (Reference 1). In 1950 Hamming devised a practical scheme of coding to effect these error-reducing properties (Reference 6). He introduced the error-detecting parity bit for a binary sequence and added bits to these for error-correcting purposes. Since 1950, numerous papers have been written on the subject of coding theory. Viterbi utilized these theories in calculating error probability as a function of the signal energy per bit for various degrees of coding (Reference 7).

With the entry of the United States into space exploration, the need for a lightweight low-power telemetry system developed. Such a system (Reference 8), utilizing the noise-reducing properties of frequency modulation and the error-reducing properties of pulse-code modulation, was incorporated in the first Vanguard scientific space vehicle and ultimately achieved orbit in Vanguard III

*P. M. Rainey, U. S. patent 1,608,527, November 30, 1926, issued to Western Electric Co., Inc.

(1959 $\eta 1$). The telemetry encoder had a 48 channel capability, weighed 6 ounces unpotted, and required 12 milliwatts of power. Pulse-frequency modulation, as the system was called, was used again on the Ionosphere Direct Measurements Satellite, Explorer VIII (1960 $\xi 1$). In April 1961 the space probe Explorer X (1961 $\kappa 1$), which measured the interplanetary magnetic field, was sent to an altitude of 240,000 km and again pulse-frequency modulation provided the encoding technique. Since that time, four more scientific satellites have been orbited with pulse-frequency-modulation telemeters. Explorer XII (1961 $\upsilon 1$) provided continuous measurements of the energetic particles in the Van Allen radiation belts out to 80,000 km; Ariel I (1962 $\sigma 1$) was an ionospheric satellite (a joint effort between the United States and the United Kingdom); Explorer XIV (1962 $\beta\gamma 1$) was a follow-on to Explorer XII; and Explorer XV (1962 $\beta\lambda 1$) is providing a study of the artificial radiation belt. Two satellites to be launched in the near future, the Interplanetary Monitoring Probe and the successor to Ariel I, will use pulse-frequency modulation as the encoding technique.

CHARACTERISTICS OF PULSE-FREQUENCY MODULATION

General Description

Consider a time function $f_1(t)$ which is band-limited between zero and $1/2T_0$ cps. The function may be completely described by a series of impulses of separation T_0 and area $f_1(nT_0)$, with $n = -\infty, \cdots, -2, -1, 0, 1, 2, \cdots, +\infty$. A sequence of these time samples may be encoded for transmission over a telemetry link in several ways. The method considered here is to encode the magnitude of the area of each impulse as the frequency of a pulsed subcarrier, the duration of the pulse being some fraction of the sample time T_0.

A set of k analog time functions $f_m(t)$ may be multiplexed by sequentially sampling each function with spacings between samples of T_0/k. In order that the spectrum may be utilized more efficiently, each pulse length should be equal to the sampling time, T_0/k. In practice the pulse length has been set at half this value to allow for response-time limitations in the crystal filters used in the detection process. Thus, a train of sequential pulses, the frequency of each being proportional to the amplitude of a sample, comprises the basic configuration for pulse-frequency modulation.

The signals $f_m(t)$ may not necessarily be analog in nature. A sizable portion of the outputs of experiments aboard spacecraft occur as digital signals, and from a signal-to-noise-ratio viewpoint it is desirable to retain the digital character of the signal. The binary digits of the signal are combined and presented as a single digit of a higher order base. The present state of the art of PFM telemetry employs the encoding of three bits as one digit to the base eight; that is, three binary digits are encoded as one of eight frequencies. A special digital pulsed-subcarrier oscillator has been developed for this purpose; it is restricted to oscillation at only one of the eight possible frequencies, the frequency depending on the value of its three-bit input. In this manner the complexity of the switching circuitry in the encoder is materially reduced, since readout of the accumulators and scalers is accomplished three bits at a time instead of serially. Figure 1 illustrates the manner of commutating the digital oscillator to scan the stored data in the accumulator. Pulses from the experiment are counted and stored as a binary number in the accumulator. The digital oscillator is

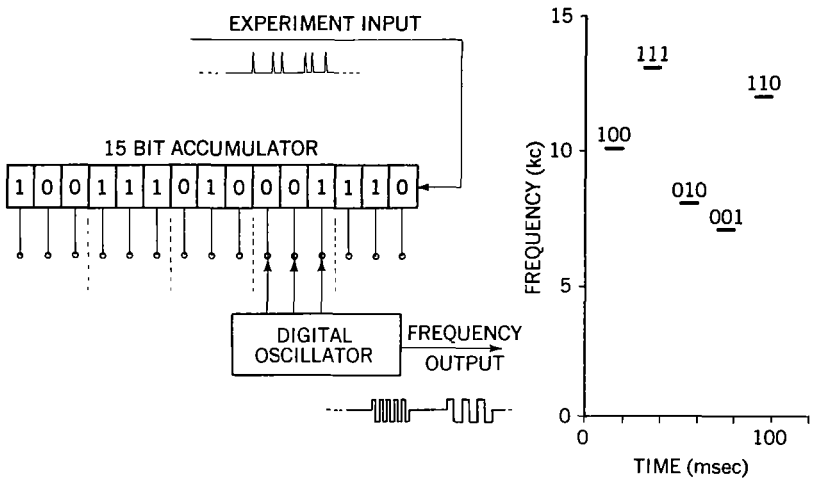

Figure 1—Digital data readout system.

commutated three bits at a time in five steps through the stored fifteen bits in the accumulator. The output of the oscillator, for this case (octal number 47216), is represented, as in Figure 1, by five serial pulses of discrete frequencies.

Since both analog and digital signals are encoded as frequencies of pulses, they may be intermixed in any order in multiplexing. Any one channel may be subcommutated to extend the number of signals $f_m(t)$ which may be encoded, with a corresponding reduction in the signal bandwidth.

The present format for PFM specifies that sixteen sequential channels comprise a telemetry frame. The first channel is devoted to synchronization, and the remaining fifteen are distributed between the analog and digital data to be telemetered. A group of sixteen sequential frames forms a telemetry sequence of 256 pulses (sixteen of these are devoted to synchronization). Figure 2 shows the frame and sequence formats.

Synchronization is assured in two ways. First, the energy in the sync pulse is increased by increasing its length 50 percent. Second, a unique frequency is utilized outside the data band for the sync pulse. To provide a means for identifying the subcommutated data, the frequency of the sync pulse in every other telemetry frame is stepped in sequence through eight frequencies. These frequencies lie in the data band and are the same as the eight frequencies of the digital oscillator. When there is a poor signal-to-noise ratio, the energy at the sync frequency may be stored over a number of frames, and thus the sync signal-to-noise ratio is improved. This, of course, increases the acquisition time but it is a necessary compromise in regions of poor signal-to-noise ratios.

Design Considerations

In the design of any telemetry system, such features as bit rate, accuracy, precision, error rate, and bandwidth must be firmly specified. Proper choices for such factors are products of the application of information theory to the problem.

Let us investigate a few factors which are necessary in a PFM telemetry system. Let the maximum value of the analog time function $f_1(t)$ be defined as the full-scale value F_1 of the channel. If F_1 is divided into N equal parts, the magnitude F_1/N represents the precision of the system. This is the smallest discernible change between two samples of $f_1(t)$. The value of N is determined by the requirements of the experiment being telemetered. For small scientific satellites a precision factor $1/N$ of 0.01, or 1 percent of the full-scale value, is normally considered adequate. For experiments, such as the flux-gate magnetometer, which depend on the measuring of the modulation of the magnetic field by the satellite's spin, precisions to 0.1 percent are desirable, although accuracy better than 1 percent is not necessary. For analog signals encoded with PFM, the precision is a function of the signal-to-noise ratio. At close range, the precision is an order of magnitude better than at maximum range. This feature, which will be discussed later in more detail, is equivalent to encoding with a variable bit-rate.

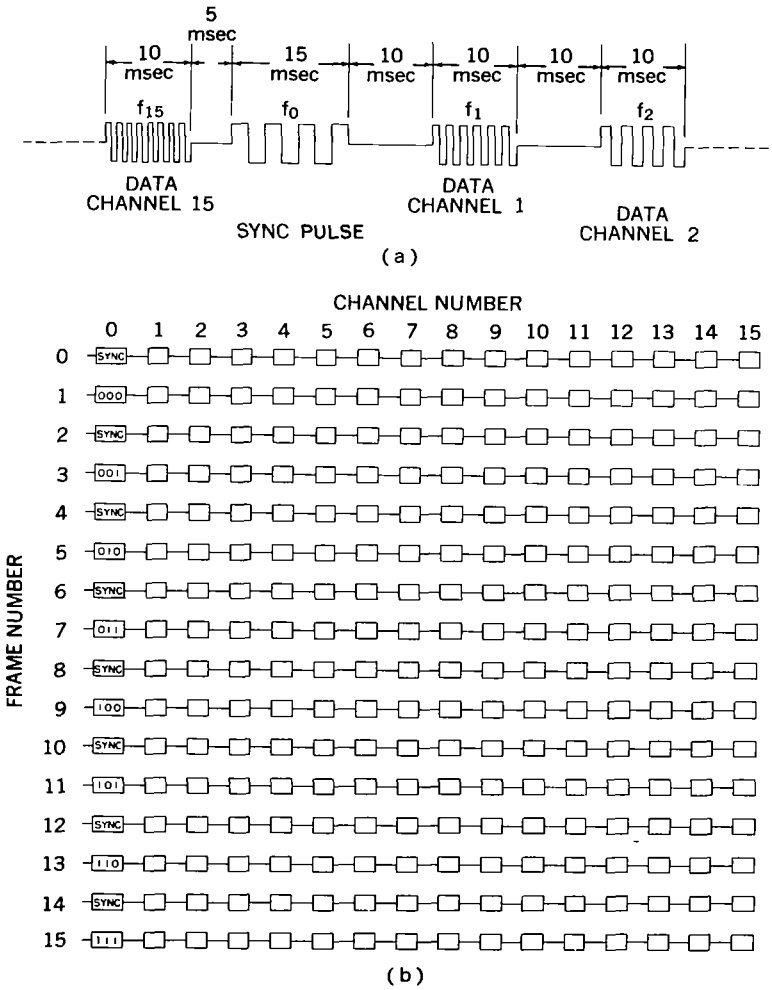

Figure 2—Pulse-frequency-modulation format:
(a) telemetry frame; (b) sequence.

Since the frequency of the pulse contains the signal information, a measurement precision of 1 percent, for example, requires that the detection system be able to discern 100 different frequencies. The total frequency band B is therefore divided into 100 equal parts. The separation between frequencies, Δf_0, is B/100. The power spectra of the pulses (Appendix A) have zeros of power density on each side of the center frequency at multiples of the reciprocal of T the pulse length. T is determined by the sampling rate necessary to telemeter the highest frequency of $f_1(t)$ at least better than at the Nyquist rate. The zeros of the power spectrum then should fall at multiples of B/100, or $\Delta f_0 = 1/T$. This gives the relation between the bandwidth, precision, and pulse length,

$$B = \frac{N}{T} , \tag{2}$$

where 1/N is the precision constant.

The above analysis was made on the basis of the sampling time of a single channel $f_1(t)$ determining the pulse length T. Since time-division multiplexing is used, the pulse length must be shortened in proportion to the number of commutated channels. Therefore the bandwidth B will increase in proportion to the number of commutated channels.

In effect, the application of Equation 2 predicts that the sample will assume any one of N, in this case 100, discrete amplitudes. The power spectrum for any one of these amplitudes is centered in one of the 100 equal parts of width Δf_0 in the band B.

A first-order solution to the detection problem is to arrange 100 contiguous bandpass filters with bandwidth $\Delta f_0 = 1/T$ to cover the bandwidth B. A maximum-likelihood detector on the outputs of the filters can select the filter with the greatest output. The signal is thus quantized into one of 100 possible levels. The original amplitude of a sample would not necessarily cause the frequency to fall exactly in the center of any one of the 100 filters. The output would still be greater in one filter than in an adjacent filter. As the amplitude of the sample is changed, the maximum-likelihood detector indicates that the adjacent filter has acquired the signal only when its response has an amplitude greater than the output of the original filter. With a good signal-to-noise ratio the filter output which is greatest can be gated into a discriminator in order that the frequency might be measured with better than 1 percent precision.

Rather than samplings only at times nT, the frequency of the pulse can be a continuous representation of the amplitude of the sample for the whole duration of the pulse, T. By using a discriminator on the output of the contiguous filters, not only can the average amplitude during the time T be determined but also the rate of change of amplitude. Having the latter information is equivalent to doubling the sampling rate (Reference 9). These topics will be discussed in detail later.

For data encoded as digital information, the minimum number of filters required in the detection system is the same as the number of frequency levels encoded. Filters for these frequency levels as well as filters contiguous to these discrete frequencies are tied together in a "greatest of" configuration as in Figure 3. This allows some latitude in the stability of each discrete frequency—temperature drift or aging of the digital oscillator might cause a discrete frequency to fall outside

its assigned filter. Thus, the "greatest of" detector selects the filter with the greatest signal and transmits to the output a digital number indicative only of the group of filters in which the signal fell.

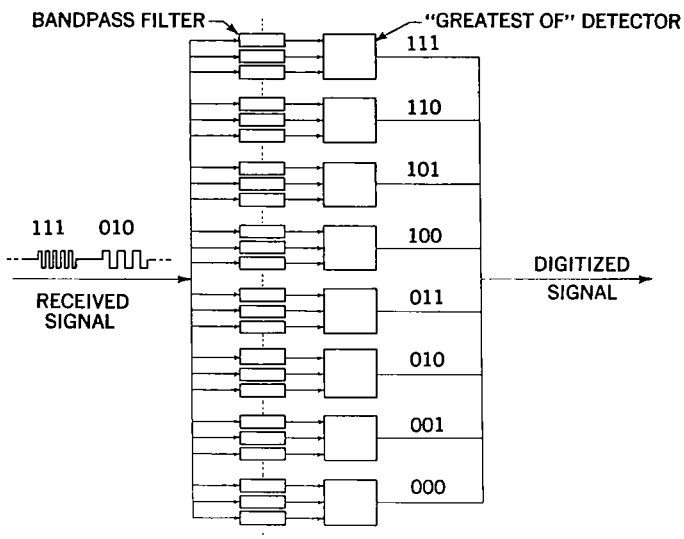

Figure 3—Contiguous-filter bank in digital-oscillator mode.

CHARACTERISTICS OF CODED BINARY SEQUENCES

A somewhat different approach to the theory of coded binary sequences will be developed in this chapter in order to illustrate the position of pulse-frequency modulation in coded telemetry. The idea is to show that PFM is a special binary code taken from a group of many codes which can be made up of patterns of binary zeros and ones.

Pulse-code modulation (PCM) is ordinarily thought of as the representation of sequential samples of a signal by a binary code; however, the original definition of PCM included all codes: binary, ternary, quaternary, etc. Patterns of these code elements make up the quantized amplitude value of the sample. For two reasons the binary code is used almost exclusively: the advantage in the signal-to-noise-ratio relation, and the ease of generation. If the amplitude of a sample is to be encoded as an n-bit binary sequence, 2^n different sequences are available to quantize the amplitude. Shannon has shown by his second theorem that the probability of error in recognizing any of the transmitted 2^n sequences may be reduced by recoding the n-bit sequences or words into selected sequences of larger m-bit sequences (Reference 1); or, conversely, if only selected sequences of the 2^n available sequences are allowed, then the probability of error per bit is reduced. Coded n-bit binary sequences are defined as a set of M selected sequences in the $M < 2^n$. When $M = 2^n$ the set of sequences is said to be uncoded.

Group Coding

Advantages may be gained by allowing the transmission of only selected sequences in the available 2^n sequences of an n-bit encoded sample. This, of course, reduces the precision to which the samples may be quantized; however, the precision may be increased back to the original value by increasing n, since this increases the number of sequences from which a judicious selection may be made. Later we shall discuss how these selections are made. A signal-to-noise advantage is obtained if the selected sequences are detected not bit-by-bit but as an entire sequence or group. Use is made of the fact that signals add directly (since their phases are correlated) and noise adds as the square root of the sum of the squares.

The detection process is accomplished by cross-correlating each of the selected or allowed sequences with the transmitted signal; the allowed sequence which yields the highest cross-correlation coefficient when correlated with the signal is selected as the most probable representation of the signal.

Let $f_l(t)$ be one of a set of k transmitted sequences and $f_m(t)$ be one of the allowed sequences stored in k correlators. Both $f_l(t)$ and $f_m(t)$ are zero for $t > T$ and $t < 0$. The correlator performs the mathematical operation:

$$\frac{n}{T} \int_0^T f_l(t + \tau)\, f_m(t)\, dt = C_{lm}(\tau) , \tag{3}$$

where

n = number of bits in the word,
T = length of sequence,
τ = lag time,
$C_{lm}(\tau)$ = unnormalized cross-correlation function.

For the matched or optimum condition the lag time should be zero. The correlator with the greatest value of $C_{lm}(0)$ is selected as the one having the greatest probability of containing the signal.

A *zero* may be represented in the transmitted signal by a +1 volt and a *one* by a -1 volt. The selected sequence or stored waveform in the correlator $f_m(t)$ is normalized so that the units of the cross-correlation coefficient $C_{lm}(0)$ will correspond to the voltage measured at the output of the correlator. When $l = m$, the cross-correlation coefficient is n volts. Since the correlator with the highest coefficient is being selected, it is desirable for the coefficient of all the other correlators to be as low as possible, so that the largest possible distinction can be made between the correct and the incorrect values of the coefficient.

As an example, let us take all the available sequences of a four-bit word and construct a truth table which gives the values of the cross-correlation coefficients of Equation 3. Table 1 contains such a table; however, the order of the four-bit words was prearranged to bring out some salient features. For $l = m$ the correlation coefficient is +4 volts; when $f_l(t)$ equals the complement of $f_m(t)$, the coefficient becomes -4 volts. In Table 1(a) there are two groups of eight sequences each. In either group the cross-correlation coefficient is zero except when the stored waveform matches the signal or is its complement. If an attempt was made to correlate signals in group 1 with the stored waveforms of group 2, the cross-correlation coefficient would be ±2 volts. Noise could easily perturb a +2 volt output into +4 volts, causing an error. Thus, if the transmitted sequences of a four-bit word are restricted entirely to either group 1 or group 2 and the stored waveforms in the correlators are of the same group, then an improvement in the signal-to-noise ratio can be realized. These code groups are of the Reed-Muller type (Reference 10).

Intuitively, if the signal-to-noise ratio were unity for a single bit of the four-bit word, the output signal-to-noise ratio would be 2/1 (the bits of the signal add directly, but the noise adds as the

Table 1

Correlation Coefficients: (a) Four-Bit Sequences; (b) One-Bit Sequences; (c) Two-Bit Sequences.

SIGNAL – $f_l(t)$

CORRELATOR – $f_m(t)$	GROUP 1 0000	0011	0101	0110	1001	1010	1100	1111	GROUP 2 0001	0010	0100	0111	1000	1011	1101	1110
GROUP 1 0000	+4	0	0	0	0	0	0	−4	+2	+2	+2	−2	+2	−2	−2	−2
0011	0	+4	0	0	0	0	−4	0	+2	+2	−2	+2	−2	+2	−2	−2
0101	0	0	+4	0	0	−4	0	0	+2	−2	+2	+2	−2	−2	+2	−2
0110	0	0	0	+4	−4	0	0	0	−2	+2	+2	+2	−2	−2	−2	+2
1001	0	0	0	−4	+4	0	0	0	+2	−2	−2	−2	+2	+2	+2	−2
1010	0	0	−4	0	0	+4	0	0	−2	+2	−2	−2	+2	+2	−2	+2
1100	0	−4	0	0	0	0	+4	0	−2	−2	+2	−2	+2	−2	+2	+2
1111	−4	0	0	0	0	0	0	+4	−2	−2	−2	+2	−2	+2	+2	+2
GROUP 2 0001	+2	+2	+2	−2	+2	−2	−2	−2	+4	0	0	0	0	0	0	−4
0010	+2	+2	−2	+2	−2	+2	−2	−2	0	+4	0	0	0	0	−4	0
0100	+2	−2	+2	+2	−2	−2	+2	−2	0	0	+4	0	0	−4	0	0
0111	−2	+2	+2	+2	−2	−2	−2	+2	0	0	0	+4	−4	0	0	0
1000	+2	−2	−2	−2	+2	+2	+2	−2	0	0	0	−4	+4	0	0	0
1011	−2	+2	−2	−2	+2	+2	−2	+2	0	0	−4	0	0	+4	0	0
1101	−2	−2	+2	−2	+2	−2	+2	+2	0	−4	0	0	0	0	+4	0
1110	−2	−2	−2	+2	−2	+2	+2	+2	−4	0	0	0	0	0	0	+4

(a)

$f_l(t)$

$f_m(t)$	0	1
0	+1	−1
1	−1	+1

(b)

$f_l(t)$

$f_m(t)$	00	01	10	11
00	+2	0	0	−2
01	0	+2	−2	0
10	0	−2	+2	0
11	−2	0	0	+2

(c)

square root of the sum of the squares). The signal-to-noise ratio has doubled and the information rate has reduced by only one-fourth. This is a good improvement; unfortunately, it cannot be realized. True, the signal-to-noise ratio out of the correlator is improved over the bit-by-bit detection, but the outputs of the correlators must be compared to determine the largest coefficient. It is probable that noise in another correlator will be greater than the coefficient in the correct correlator. This probability increases as the number of correlators increases. The situation is discussed in detail later. The group code method still provides a substantial improvement in the signal-to-noise ratio over bit-by-bit detection.

The number of correlators in group 1 can be reduced from eight to four if the −4 volt output also is utilized. Since each correlator responds only to its matched signal and its complement, a single correlator can be used to detect two sequences. The correlator with the greatest absolute magnitude is selected as the one having the best probability of containing the signal. The sign of the coefficient determines whether the signal was in the first or second four sequences of a group. A code of this type is said to be bi-orthogonal since negative as well as positive cross-correlation coefficients are utilized. When only the positive outputs are used the code is orthogonal.

In the preceding example the prearranged order of the four-bit sequences was most important. A few fundamental rules have been developed to generate codes with bit lengths of $n = 2^k$, where $k = 0, 1, 2, 3, \cdots$. These rules are amenable to computer programming but are somewhat different from those found in the literature. Consider first the correlation table for a one-bit word as in Table 1(b). Only one correlator is required if the bi-orthogonal properties of the signal are utilized. This table and the correlation table for the two-bit sequences of Table 1(c) can be written by inspection. The first word of the four-bit table is generated by combining the first word, 00, of the two-bit table with itself to form 0000. The next word is made by combining the first word, 00, with its complement, 11, to form 0011. The same process is carried out with the second word of the two-bit table to form the next two words. The complements of these four words are now taken in reverse order; this generates the code of group 1. The group 2 code is started by combining the first word of the two-bit table with the second. The next word is obtained by combining the first word of the two-bit table with the complement of the second. For the third and fourth words the two-bit second word is combined with the first word and then with its complement. The next four words are the complements of the newly generated words in reverse order.

The eight-bit correlation table has 256 sequences which form a matrix of 65,536 correlation coefficients. A digital computer program for generating the 8-bit table was written by utilizing the four-bit table and the rules for forming the table from the preceding paragraph. The program was written in FAP (Fortran Assembly Program) so that the bit patterns of the signals $f_l(t)$ and stored waveforms $f_m(t)$ could be cyclically varied. That is, the first bit of all the eight-bit sequences was moved to the last-bit position and a new set of correlation coefficients computed.

The program is arranged so that a print-out contains the correlation between the first sixteen signals and the first sixteen stored waveforms. Table 2 is a print-out of the first page of the code book for the program. On the next page are the first sixteen signals correlated with the second sixteen correlators, and so on. There are sixteen code groups of the type in Table 2. Any one of these sixteen code groups could be used to encode four bits of data for a signal-to-noise-ratio improvement over a standard four-bit code. Table 3 illustrates the correlation between groups.

It is interesting to note that a cyclic variation of the four-bit sequences does not generate any new codes. It only rearranges the order in the two code groups. In the eight-bit case, however, new codes are generated; in fact, a tremendous number of new codes can be made not only by cyclically varying the bit locations of the signal and stored waveforms but also by interchanging the order of the bits in all possible combinations.

The process may be carried to the sixteen-bit case, for which there are over 4×10^9 cross-correlation coefficients. Sanders has described the Digilock coded binary PCM telemeter, which encodes sixteen-bit words to represent five-bit samples (Reference 11). This system has been flown on an Air Force Blue Scout rocket.

Parity Codes

A simple error-detecting parity code is constructed by adding one bit to an n-bit sequence to indicate whether the total word has an even or an odd number of *zeros*. It is most interesting to

note that group 1 of the four-bit correlation table can be made from a three-bit sequence by adding an even parity bit; group 2 is generated by adding an odd parity bit. The eight-bit code of Table 2 may be thought of as a four-bit code with four bits for error-detecting and error-correcting.

PFM Correlation Table

In the eight-bit correlation table (Table 2) the second sequence, 00001111, is the same as the second sequence of the four-bit table of Table 1(a), 0011, if the words of each are of the same duration. The second word of the two-bit table of Table 1(c), 01, is also the same as these two if the time T for the words is the same. Since identical words can be found on different correlation tables, the possibility might be considered that a new table could be constructed from sequences taken from a number of tables. These sequences should have orthogonal properties. The most obvious one is

Table 2

Correlation Coefficients for Bi-Orthogonal Code Group.

		1	2	3	4	5	6	7	8	9	10	11	12	13	14	15	16
		0	0	0	0	0	0	0	0	1	1	1	1	1	1	1	1
		0	0	0	0	1	1	1	1	0	0	0	0	1	1	1	1
		0	0	1	1	0	0	1	1	0	0	1	1	0	0	1	1
		0	0	1	1	1	1	0	0	1	1	0	0	0	0	1	1
		0	1	0	1	0	1	0	1	0	1	0	1	0	1	0	1
		0	1	0	1	1	0	1	0	1	0	1	0	0	1	0	1
		0	1	1	0	0	1	1	0	1	0	0	1	1	0	0	1
		0	1	1	0	1	0	0	1	0	1	1	0	1	0	0	1
1	00000000	8	0	0	0	0	0	0	0	0	0	0	0	0	0	0	-8
2	00001111	0	8	0	0	0	0	0	0	0	0	0	0	0	0	-8	0
3	00110011	0	0	8	0	0	0	0	0	0	0	0	0	0	-8	0	0
4	00111100	0	0	0	8	0	0	0	0	0	0	0	0	-8	0	0	0
5	01010101	0	0	0	0	8	0	0	0	0	0	0	-8	0	0	0	0
6	01011010	0	0	0	0	0	8	0	0	0	0	-8	0	0	0	0	0
7	01100110	0	0	0	0	0	0	8	0	0	-8	0	0	0	0	0	0
8	01101001	0	0	0	0	0	0	0	8	-8	0	0	0	0	0	0	0
9	10010110	0	0	0	0	0	0	0	-8	8	0	0	0	0	0	0	0
10	10011001	0	0	0	0	0	0	-8	0	0	8	0	0	0	0	0	0
11	10100101	0	0	0	0	0	-8	0	0	0	0	8	0	0	0	0	0
12	10101010	0	0	0	0	-8	0	0	0	0	0	0	8	0	0	0	0
13	11000011	0	0	0	-8	0	0	0	0	0	0	0	0	8	0	0	0
14	11001100	0	0	-8	0	0	0	0	0	0	0	0	0	0	8	0	0
15	11110000	0	-8	0	0	0	0	0	0	0	0	0	0	0	0	8	0
16	11111111	-8	0	0	0	0	0	0	0	0	0	0	0	0	0	0	8

Table 3

Cross-Correlation Coefficients for Eight-Bit Sequences.

		33	34	35	36	37	38	39	40	41	42	43	44	45	46	47	48
		0	0	0	0	0	0	0	0	1	1	1	1	1	1	1	1
		0	0	0	0	1	1	1	1	0	0	0	0	1	1	1	1
		0	0	1	1	0	0	1	1	0	0	1	1	0	0	1	1
		0	0	1	1	1	1	0	0	1	1	0	0	0	0	1	1
		0	1	0	1	0	1	0	1	0	1	0	1	0	1	0	1
		1	0	1	0	0	1	0	1	0	1	0	1	1	0	1	0
		0	1	1	0	0	1	1	0	1	0	0	1	1	0	0	1
		1	0	0	1	0	1	1	0	1	0	0	1	0	1	1	0
113	00000111	6	2	2	-2	-2	2	2	-2	2	-2	-2	2	2	-2	-2	-6
114	00001000	2	6	-2	2	2	-2	-2	2	-2	2	2	-2	-2	2	-6	-2
115	00110001	2	-2	2	6	2	-2	2	-2	2	-2	2	-2	-6	-2	2	-2
116	00111110	-2	2	6	2	-2	2	-2	2	-2	2	-2	2	-2	-6	-2	2
117	01010010	-2	2	2	-2	6	2	2	-2	2	-2	-2	-6	2	-2	-2	2
118	01011101	2	-2	-2	2	2	6	-2	2	-2	2	-6	-2	-2	2	2	-2
119	01100100	2	-2	2	-2	2	-2	2	6	-6	-2	2	-2	2	-2	2	-2
120	01101011	-2	2	-2	2	-2	2	6	2	-2	-6	-2	2	-2	2	-2	2
121	10010100	2	-2	2	-2	2	-2	-6	-2	2	6	2	-2	2	-2	2	-2
122	10011011	-2	2	-2	2	-2	2	-2	-6	6	2	-2	2	-2	2	-2	2
123	10100010	-2	2	2	-2	-2	-6	2	-2	2	-2	6	2	2	-2	-2	2
124	10101101	2	-2	-2	2	-6	-2	-2	2	-2	2	2	6	-2	2	2	-2
125	11000001	2	-2	-6	-2	2	-2	2	-2	2	-2	2	-2	2	6	2	-2
126	11001110	-2	2	-2	-6	-2	2	-2	2	-2	2	-2	2	6	2	-2	2
127	11110111	-2	-6	2	-2	-2	2	2	-2	2	-2	-2	2	2	-2	6	2
128	11111000	-6	-2	-2	2	2	-2	-2	2	-2	2	2	-2	-2	2	2	6

to take 01010101 from the eight-bit table, 0101 from the four-bit table, and 01 from the two-bit table and construct a new table. From a six-bit table we could use 010101. All of these sequences are orthogonal to each other when substituted into Equation 3. Also, the alternating *zero* and *one* code may be taken from higher order tables in constructing this new table. Pulse frequency modulation does exactly this in constructing a code. The code is made up of alternating *zeros* and *ones* taken from higher order codes. For PFM signals in the frequency range from 5 to 15 kc, the 5.0 kc sequence would be 100 bits of 50 *zeros* and 50 *ones* in an alternating pattern; the 5.1 kc sequence would be 102 bits in this same alternating pattern. Table 4 is such a table. Each frequency contains an integral number of cycles because the pulse length, derived from Equation 3, is constant. The

Table 4

Pulse-Frequency-Modulation Correlation Table.

CORRELATOR FREQUENCY (kc) \ SIGNAL FREQUENCY (kc)	5.0	5.1	5.2	5.3	.....	14.7	14.8	14.9	15.0
5.0	100	0	0	0	.....	0	0	0	0
5.1	0	102	0	0	.....	0	0	0	0
5.2	0	0	104	0	.....	0	0	0	0
5.3	0	0	0	106	.....	0	0	0	0
.....	.....	.....	.....	.....	.....	.....	.....	.....	.....
14.7	0	0	0	0	.....	294	0	0	0
14.8	0	0	0	0	.....	0	296	0	0
14.9	0	0	0	0	.....	0	0	298	0
15.0	0	0	0	0	.....	0	0	0	300

table is strictly an orthogonal code. If the sequences starting with a *one* instead of a *zero* were also used, the code would become bi-orthogonal, since negative values of the cross-correlation coefficient would result. Finally, if the frequencies of PFM are restricted to a set containing an integral number of cycles, then it appears that PFM is certainly a form of coded binary PCM. Of course, it is a special group code, chosen primarily because of its ease of generation.

NOISE ANALYSIS

In the previous section pulse-frequency modulation was exemplified by a special set of binary coded sequences which were selected because of their ease of generation. Of primary interest are the characteristics of this code set in the presence of noise. A number of methods are available to aid in recovering the signal set from noise. The optimum method is to use matched filters with maximum-likelihood detection. The number of filters employed is a function of the desired efficiency of encoding; n-bit precision for a single word requires 2^{n-1} filters. The matched-filter technique has been well reported (References 12 and 13). The idea is to force the power spectrum of the impulsive response of the filter to be identical to the power spectrum of the signal. Although the use of matched filters is most desirable, there are numerous situations in which the use of unmatched

filters can markedly reduce hardware and implementation complexity without too great a degradation in the signal-to-noise ratio. The noise analyses differ, depending on whether the filter in the detection system is matched or unmatched.

Unmatched Filter

The use of unmatched filters for PFM signals in which the number of quantized levels exceeds eight ($n = 3$) can simplify the operation of the detection system, compared with the use of a matched-filter set. The unmatched-filter set would consist of N contiguous bandpass filters, where N is the number of quantized levels in the signal.

Let us examine one of these filters in detail. Assume the filter to have the following power spectrum:

$$\left.\begin{aligned} K(\omega) &= 0 \quad \text{for } \omega < \left(\omega_0 - \frac{\Delta\omega_0}{2}\right), \\ K(\omega) &= 1 \quad \text{for } \left(\omega_0 - \frac{\Delta\omega_0}{2}\right) < \omega < \left(\omega_0 + \frac{\Delta\omega_0}{2}\right), \\ K(\omega) &= 0 \quad \text{for } \omega > \left(\omega_0 + \frac{\Delta\omega_0}{2}\right), \end{aligned}\right\} \tag{4}$$

where $\Delta\omega_0$ is the bandwidth of the filter and ω_0 is the center frequency of the filter.

White additive Gaussian noise with a power density of N_0 watts/cps will have a variance of σ^2 watts in the output when passed through this filter. The noise output of a narrow-band filter may be represented by using inphase and quadrature components:

$$u(t) = x(t) \cos \omega_0 t + y(t) \sin \omega_0 t \ , \tag{5}$$

where $x(t)$ and $y(t)$ are random variables.

Neither the $x(t)$ nor $y(t)$ frequency spectrum extends up to the center frequency ω_0. The mean-square-deviation or variance σ^2 is the sum of the variances of the inphase and quadrature components, $\sigma^2 = \sigma_I^2 + \sigma_Q^2$ (the covariance between the inphase and quadrature components is zero); also $\sigma^2 = \sigma_x^2/2 + \sigma_y^2/2$, where σ_x^2 and σ_y^2 are the variances of $x(t)$ and $y(t)$.

It would be rare indeed for a filter to have infinite slope on its band edges. This postulates a filter having an infinite number of sections with infinite delay time; however, a simple RLC single-pole filter serves as the first approximation to this ideal filter. The following analysis will involve only the ideal filter.

Ideal Filter

Consider a single ideal filter of bandwidth $\Delta\omega$ and center frequency ω_0. In the presence of N_0 watts/cps of noise on the input, the output power measured in a matched 1 ohm load would be $N_0 \Delta\omega/2\pi$

or σ^2 watts. If a step sinusoidal voltage of amplitude C_0 and frequency ω_0 is added to the input, the correct prediction of whether or not the signal is present after a period T has elapsed is a matter of statistics. The sinusoidal signal will be termed a "word," and the probability of incorrectly assuming the presence of a signal will be termed the "word-error probability."

Although the noise output of the filter cannot be predicted, certain probabilities may be assigned to the noise characteristics in order to evaluate the long-term effect of the presence of the noise. Some of these characteristics are the first and second moments of the noise, the probability of the rate of zero crossings, and the envelope probability density function. For the unmatched-filter case this report will be concerned mainly with the probability density function of the envelope amplitude of the noise output, since an uncorrelated detector produces a voltage proportional to the envelope of its input.

The amplitude of the noise in the output of the unmatched filter, like that in the input, has a Gaussian probability density function. Positive and negative amplitudes are equiprobable, zero being the most probable value. The autocorrelation function $\phi_{11}(\tau)$ of the input noise extending to the upper frequency limit ω_c is

$$\phi_{11}(\tau) = \lim_{T \to \infty} \frac{1}{T} \int_0^T u(t)\, u(t+\tau)\, dt \quad . \tag{6}$$

From theorem 202 in Reference 14

$$\phi_{11}(\tau) = \lim_{T \to \infty} \frac{1}{2\pi} \int_{-\infty}^{\infty} \frac{|F(\omega)|^2}{T} e^{i\omega\tau}\, d\omega \quad , \tag{7}$$

where

$$F(\omega) = \int_{-\infty}^{\infty} u(t)\, e^{-i\omega t}\, dt \quad .$$

Then

$$\phi_{11}(\tau) = \frac{1}{2\pi} \int_{-\infty}^{\infty} \frac{P(\omega)}{2} e^{i\omega\tau}\, d\omega \quad , \tag{8}$$

since

$$\lim_{T \to \infty} \frac{|F(\omega)|^2}{T} = \frac{P(\omega)}{2} \quad ,$$

where $P(\omega)$ is the power spectrum of $u(t)$. But $P(\omega) = N_0$ watts/cps and

$$\phi_{11}(\tau) = \frac{N_0}{2}\int_{-\omega_c}^{\omega_c} e^{i\omega\tau}\,\frac{d\omega}{2\pi}$$

$$= \frac{N_0\,\omega_c}{2\pi}\,\frac{\sin\omega_c\tau}{\omega_c\tau} \quad . \tag{9}$$

The autocorrelation function is periodic as τ is increased, the correlation damping out approximately as a $1/\tau$ function. As ω_c approaches infinity $\phi_{11}(\tau)$ becomes an impulse function centered at $\tau = .0$:

$$\lim_{\omega_c \to \infty} \phi_{11}(\tau) = \lim_{\omega_c \to \infty} \frac{1}{2\pi}\int_{-\omega_c}^{\omega_c} \frac{N_0}{2}\,e^{i\omega\tau}\,d\tau$$

$$= \frac{N_0}{2}\,\delta(\tau) \quad , \tag{10}$$

where

$$\int_{-\infty}^{\infty} \delta(\tau)\,d\tau = 1 \quad .$$

For the output of the bandpass filter $(\omega_c >> \omega_0)$ the autocorrelation function for Gaussian noise becomes (Appendix B)

$$\phi_{11}(\tau) = N_0\,\frac{\Delta\omega}{2\pi}\,\frac{\sin\frac{\Delta\omega\tau}{2}}{\frac{\Delta\omega\tau}{2}}\cos\omega_0\tau \quad . \tag{11}$$

The function is plotted in Figure 4. The output of the filter tends to exhibit periodic correlation until the lag time $\tau_0 = 2\pi/\Delta\omega$ is reached. Let $n(t)$ be the noise voltage output and e_d the detector voltage output. When the output of the filter is passed through a simple detector with the characteristics

$$\left.\begin{aligned} e_d &= -n(t) \quad \text{for } n(t) \le 0 \ , \\ e_d &= +n(t) \quad \text{for } n(t) \ge 0 \ , \end{aligned}\right\} \tag{12}$$

full-wave rectification of the output occurs. Smoothing of this rectified output yields $\sqrt{|x(t)|^2 + |y(t)|^2}$, the amplitude of the envelope of $u(t)$ (Equation 5).

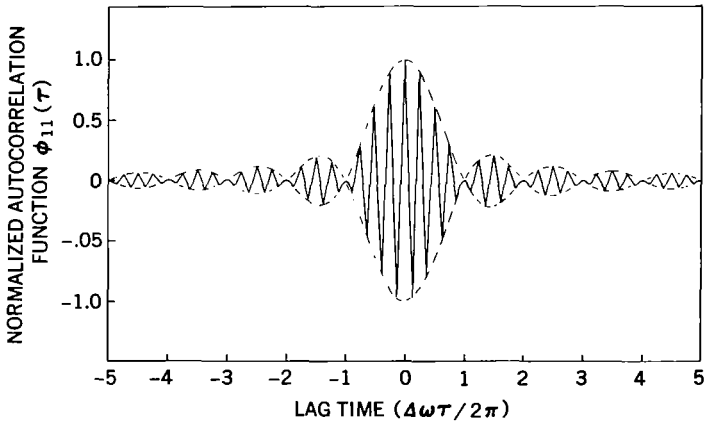

Figure 4—Autocorrelation function for Gaussian noise $(\omega_0 = 4\Delta\omega)$.

Of great interest is the joint probability density function for the amplitudes of $x(t)$ and $y(t)$. Since $x(t)$ and $y(t)$ are equiprobable, have a normal distribution, and are statistically independent, they may be conveniently plotted on orthogonal coordinates with the z axis representing the joint probability, as in Figure 5. The amplitude at the point x_1, y_1 represents the probability density of the joint occurrence of the amplitude x_1 at the same time as the quadrature amplitude y_1. The distance from the center to this point is $\sqrt{x_1^2 + y_1^2}$; however, other values of x and y with the same square-sum value lie on the circle with radius $\sqrt{x_1^2 + y_1^2}$. This circle is the locus of points of constant probability density for the amplitude of the envelope of the noise. To show this the variables must be changed from rectangular coordinates x and y to polar coordinates r and θ.

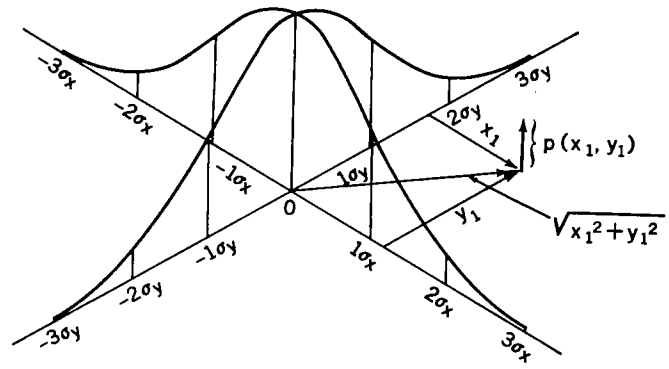

Figure 5—Joint probability density function for Gaussian noise.

The probability density for the joint occurrence of x_1 and y_1 is:

$$p(x_1, y_1) = \frac{1}{\sqrt{2\pi}\,\sigma_x} e^{-x_1^2/2\sigma_x^2} \frac{1}{\sqrt{2\pi}\,\sigma_y} e^{-y_1^2/2\sigma_y^2}$$

$$= \frac{1}{2\pi\sigma_x\,\sigma_y} e^{-\frac{1}{2}\left(x_1^2/\sigma_x^2 + y_1^2/\sigma_y^2\right)} . \qquad (13)$$

Now $x = r\cos\theta$ and $y = r\sin\theta$. The Jacobian is

$$\left| t_{\bar{k}}^{k} \right| = \begin{vmatrix} \frac{\partial x}{\partial r} & \frac{\partial y}{\partial r} \\ \frac{\partial x}{\partial \theta} & \frac{\partial y}{\partial \theta} \end{vmatrix}$$

$$= \begin{vmatrix} \cos\theta & \sin\theta \\ -r\sin\theta & r\cos\theta \end{vmatrix}$$

$$= r .$$

The joint probability for r and θ is then

$$p(r,\theta) = \left| t_{\bar{k}}^{k} \right| p(x,y)$$

$$= \frac{r}{2\pi\sigma_x\,\sigma_y} e^{-\frac{1}{2}\left(r^2\cos^2\theta/\sigma_x^2 + r^2\sin^2\theta/\sigma_y^2\right)} . \qquad (14)$$

In the present case $\sigma_x = \sigma_y$, so

$$p(r,\theta) = \frac{r}{2\pi\sigma_x^2} e^{-r^2/2\sigma_x^2} . \tag{15}$$

The probability for any value of θ is

$$p(r) = \int_0^{2\pi} p(r,\theta)\, d\theta$$

$$= \frac{r}{\sigma_x^2} e^{-r^2/2\sigma_x^2} . \tag{16}$$

This is the Rayleigh distribution which describes the probability of obtaining a specified amplitude of the envelope of bandwidth-limited random noise.

Rayleigh noise is characterized by a probability which is zero for zero envelope amplitude, a maximum for amplitude equal to the deviation, and low for large amplitudes.

Word-Error Probability for the Unmatched Filter

The addition of a sinusoidal signal to the noise causes a shift in the envelope probability density function, as shown by Rice (Reference 15). Adding a sine wave carrier of amplitude A_0 displaces the probability density function a distance of A_0 units along the x axis. In the limit, as the variance of the noise approaches zero the probability density function for the envelope approaches an impulse at $x = A_0$. The volume under this impulse is unity, so the probability of an amplitude other than A_0 is zero. Adding a cosine of amplitude B_0 shifts the center to $\sqrt{A_0^2 + B_0^2}$ at an angle $\theta_0 = \tan^{-1}(B_0/A_0)$ to the x axis. Figure 6 depicts this general case. The volume above any area of the x-y plane gives the probability of the envelope having an amplitude falling in the region of that x-y area.

However, we are mainly interested in constant envelope amplitudes with unknown phases since they characterize a typical PFM signal. The probability of an amplitude lying between r and $r + dr$ (when $dr = \sqrt{dx^2 + dy^2}$) is the volume of the ring of radius r and width dr; the height is given by the joint probability density between x and y. The volume in the clear segment of Figure 6 gives this probability:

$$p(r) = \int_0^{2\pi} \frac{1}{\sqrt{2\pi}\,\sigma_x} e^{-(r\cos\theta - A_0)^2/2\sigma_x^2} \frac{1}{\sqrt{2\pi}\,\sigma_y} e^{-(r\sin\theta - B_0)^2/2\sigma_y^2} r\, dr\, d\theta . \tag{17}$$

Rice has compiled the probability curves for various carrier amplitudes (Reference 15).

The probability that an envelope amplitude will be equal to or less than r is given by the volume inside the circle of radius r_0:

$$P(r < r_0) = \int_0^{r_0} \int_0^{2\pi} \frac{1}{\sqrt{2\pi}\,\sigma_x} e^{-(r\cos\theta - A_0)^2/2\sigma_x^2} \frac{1}{\sqrt{2\pi}\,\sigma_y} e^{-(r\sin\theta - B_0)^2/2\sigma_y^2} r\, d\theta\, dr .$$

When $\sigma_x = \sigma_y$,

$$P(r < r_0) = \int_0^{r_0} \int_0^{2\pi} \frac{r}{2\pi\sigma_x^2} e^{-\left[r^2(\cos^2\theta + \sin^2\theta) - 2r(A\cos\theta + B\sin\theta) + A_0^2 + B_0^2\right]/2\sigma_x^2} d\theta\, dr ,$$

$$= \frac{1}{\sigma_x^2} \int_0^{r_0} r\, e^{-(r^2 + A_0^2 + B_0^2)/2\sigma_x^2} \frac{1}{2\pi} \int_0^{2\pi} e^{r(A_0\cos\theta + B_0\sin\theta)/\sigma_x^2} d\theta\, dr . \qquad (18)$$

Let $A_0 = C_0 \cos\theta_0$ and $B_0 = C_0 \sin\theta_0$. Then

$$P(r < r_0) = \frac{1}{\sigma_x^2} \int_0^{r_0} r\, e^{-(r^2 + C_0^2)/2\sigma_x^2} \frac{1}{2\pi} \int_0^{2\pi} e^{r C_0 \cos(\theta - \theta_0)/\sigma_x^2} d\theta\, dr . \qquad (19)$$

The second integral in the preceding equation is the modified Bessel function $I_0(r)$.

We have examined the action of an individual ideal bandpass filter and, given signal-with-noise input, have determined the probability of a particular output. Now let us look at the action of signal and noise as an input to a bank of parallel bandpass filters (the band edges of the filters are touching).

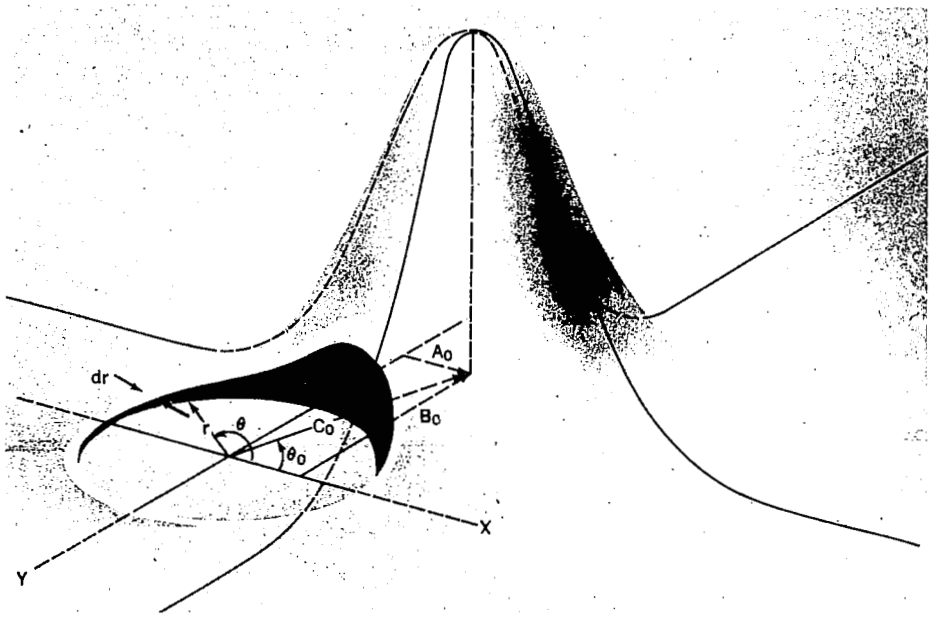

Figure 6—Joint probability density function for signal plus Gaussian noise.

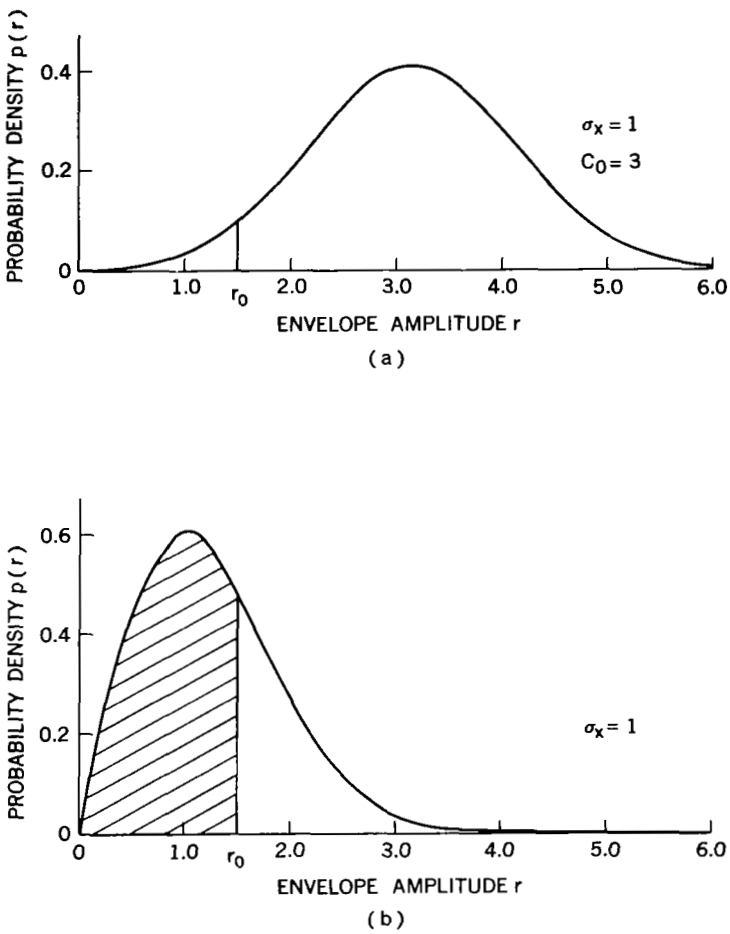

Figure 7—Probability density functions: (a) signal plus Rayleigh noise; (b) Rayleigh noise.

With N filters, a frequency range of $N\Delta\omega/2\pi$ is covered. It should be remembered that the primary advantage of PFM is that each PFM word is orthogonal to any other word in that PFM set. This gives a uniqueness to the power spectrum of each word, resulting in a bandwidth equal to the products of the number of words in the PFM set and the bandwidth of the power spectrum of a word.

Consider a PFM word and white additive Gaussian noise as an input to the bank of filters. The sinusoidal frequency of the word lies in the center of one of the N bandpass filters; the probability density function for that filter will appear as in Figure 7(a). The remaining N-1 filters will have a probability density function as given in Figure 7(b). Ultimately we are looking for a number which represents the ratio of the number of times that noise in one or more of the N-1 filters is greater than the signal-plus-noise in the correct filter. This figure is defined as the word-error probability.

It is interesting to consider some of the aspects of those things which influence the word-error probability. First, with N filters in parallel and the outputs connected in a "greatest of" configuration, the probability that at least one of the N filters will exceed a certain amplitude r_0 is almost N times the probability that a single filter output will exceed that amplitude. For example, for a bank of 100 filters with a threshold set on the "greatest of" output of 3 times the average noise voltage of a single filter, the number of times that this level is exceeded by any filter is less than 100 times the average rate a single filter will exceed that amplitude. The reason the rate is not exactly 100 times greater is the finite probability that two (or more) of the filters may simultaneously exceed the threshold. In Figure 7(b) the shaded area represents the probability that the envelope amplitude of one filter is less than the threshold amplitude r_0. The probability that all the filters, except the one with the signal, have amplitudes less than r_0 is $P(r < r_0)^{N-1}$. The probability that at least one of the amplitudes is greater than r_0 then becomes $1 - [P(r < r_0)]^{N-1}$. By increasing the signal an amount Δr_0, the error rate becomes the same for N-1 filters as for a single filter. From this increase of r_0 by the amount Δr_0, the following equality can be set up:

$$1 - P(r < r_0) = 1 - \left[P(r < r_0 + \Delta r_0)\right]^{N-1} . \qquad (20)$$

The fact that the signal amplitude would also be increased by an amount Δr_0 is more than compensated for by the increase of the information rate by $\log_2 100$ over that of a single filter. In order to keep the information rate constant, the bandwidth of each of the N filters can be reduced by the factor $1/\log_2 100$, which substantially decreases the signal power needed to maintain the same word-error probability at the same information rate.

The calculation of the word-error-probability curves for a set of 2^n uncorrelated filter outputs may proceed generally as above; i.e., the probability that an output is correct is calculated and then subtracted from unity for the probability of error. The probability of one of the N-1 filters having an amplitude equal to or less than the envelope amplitude r_0 of the filter containing the signal is given by

$$P(r < r_0) = \frac{1}{\sigma_x^2} \int_0^{r_0} r\, e^{-r^2/2\sigma_x^2}\, dr . \tag{21}$$

However, the probability that noise amplitude in any one of the N-1 filters does not exceed r_0 is the probability distribution function raised to the N-1 power. The probability that the signal-plus-noise in the correct filter has the amplitude r_0 is

$$p(r_0) = \frac{r_0}{\sigma_x^2}\, e^{-\left(r_0^2 + c_0^2\right)/2\sigma_x^2}\, \frac{1}{2\pi} \int_0^{2\pi} e^{r_0 c_0 \cos\left(\theta - \theta_0\right)/\sigma_x^2}\, d\theta . \tag{22}$$

Then, the joint probability that none of the N-1 filters has noise exceeding r_0 and that the signal-plus-noise in the correct filter has the amplitude r_0 is

$$P_c(N) = \left(\frac{1}{\sigma_x^2} \int_0^{r_0} r\, e^{-r^2/2\sigma_x^2}\, dr\right)^{N-1} \frac{r_0}{\sigma_x^2}\, e^{-\left(r_0^2 + c_0^2\right)/2\sigma_x^2}\, \frac{1}{2\pi} \int_0^{2\pi} e^{r_0 c_0 \cos\left(\theta - \theta_0\right)/\sigma_x^2}\, d\theta\, dr_0 . \tag{23}$$

For the total probability that the amplitude of the correct filter is always greater than any amplitude in the N-1 filters, the integration is performed over all values of r_0 from zero to infinity. The word-error probability is then 1 minus this quantity:

$$P_e(N) = 1 - \int_0^{\infty} \left(\frac{1}{\sigma_x^2} \int_0^{r_0} r\, e^{-r^2/2\sigma_x^2}\, dr\right)^{N-1} \frac{r_0}{\sigma_x^2}\, e^{-\left(r_0^2 + c_0^2\right)/2\sigma_x^2}\, \frac{1}{2\pi} \int_0^{2\pi} e^{r_0 c_0 \cos\left(\theta - \theta_0\right)/\sigma_x^2}\, d\theta\, dr_0 . \tag{24}$$

This equation was programmed on an IBM 7090 digital computer for various numbers of filters; the resulting curves are shown in Figure 8. The value of n in the figure is equivalent to $\log_2 N$ in Equation 24. This notation was used so that direct comparisons could be made with Viterbi's curves for "greatest of" detectors using matched filters (Reference 7).

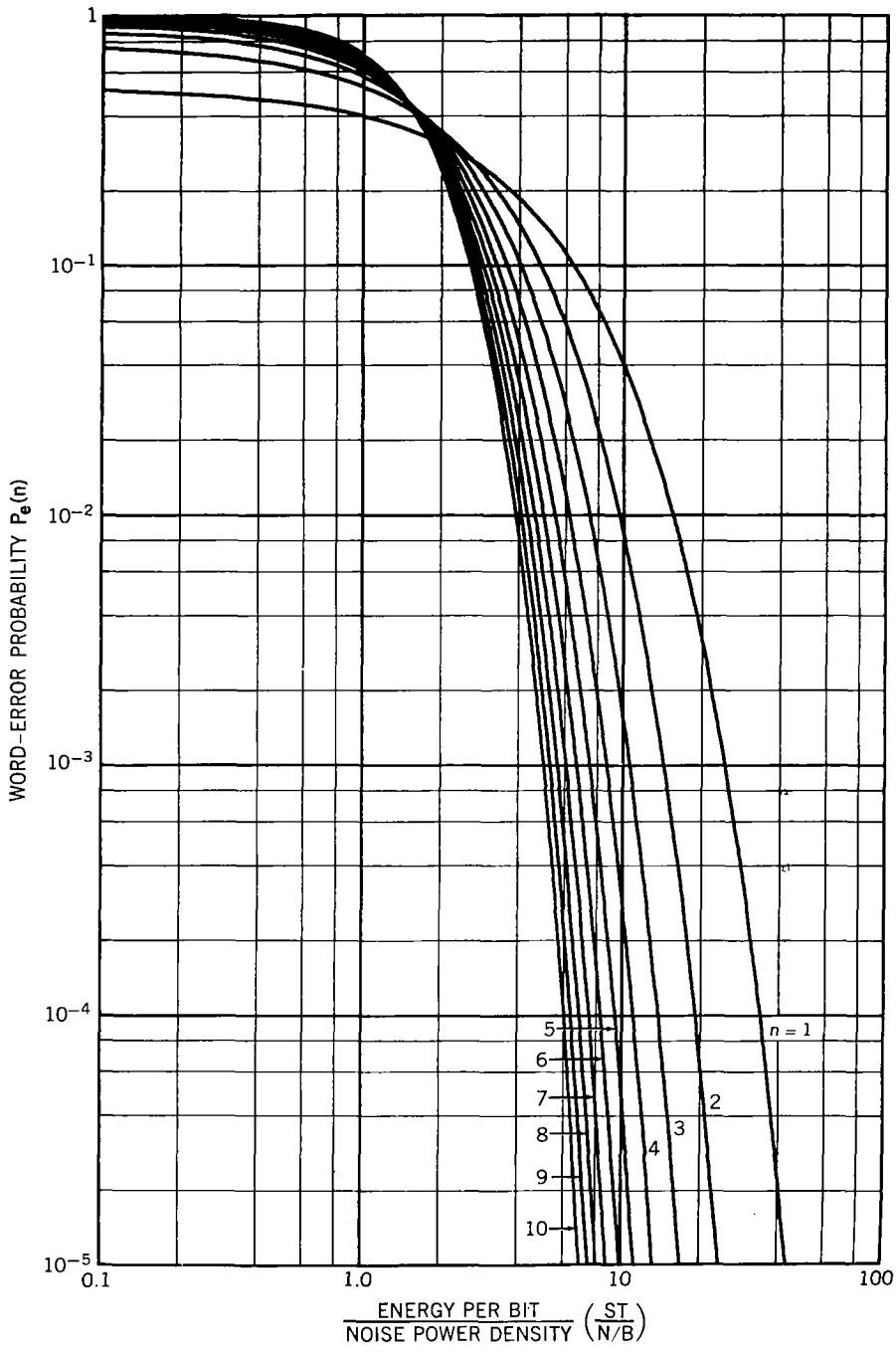

Figure 8—Word-error probability curves for Rayleigh noise.

Matched Filter

It was stated for the case of the unmatched filter that a bandpass filter is the first approximation to a matched filter for a pulsed sine wave, $C_0 \sin \omega_0 t\left[u(t) - u\left(t - T_0\right)\right]$. A matched filter is one which yields the maximum signal-to-noise ratio at a time $t = T_0$ for a given signal at the input

accompanied with additive white Gaussian noise. Several excellent treatments are available in the literature for the proof of this (Reference 16). The transfer function of the matched filter is proportional to the complex conjugate of the spectrum of the signal, $S^*(\omega)$:

$$k(\omega) = e^{-i\omega T_0} S^*(\omega) .$$

The factor $e^{-i\omega T_0}$ is the complex shifting function and corresponds to the delay time of the filter.

Multiple Matched Filter

Essentially, a matched filter performs the process of cross-correlating the signal-plus-noise with a stored matching signal. This process is actually autocorrelation of the signal with the stored image of the signal in the matched filter. The cross-correlation function,

$$\frac{1}{T_0} \int_0^{T_0} f_l(t)\, f_m(t + \tau)\, dt ,$$

is a maximum for $l = m$ when $\tau = 0$. If other signals are added to the set such that

$$\frac{1}{T_0} \int_0^{T_0} f_l(t)\, f_m(t)\, dt = 0 \quad \text{for } l \neq m , \tag{25}$$

then any one filter in the set of matching filters will respond to only one signal in the set; i.e.,

$$\frac{1}{T_0} \int_0^{T_0} f_l(t)\, f_m(t)\, dt = 0 \quad \text{for } l \neq m ,$$

and

$$\frac{1}{T_0} \int_0^{T_0} f_l(t)\, f_m(t)\, dt = C_{l\,m} \quad \text{for } l = m .$$

By observing the outputs of the filters when $\tau = 0$ (maximum autocorrelation), a probability can be established that the matched filter with the greatest output contains the signal. The error probability is, then, 1 minus the probability of being correct.

The waveform for the set of signals $f_l(t)$ has not been given. It is possible to use any orthonormal set, such as Legendre polynomials, Bessel functions, elliptic functions, or sine functions. PFM is based on the use of a set of sine functions having orthonormal properties. The time-limited sine wave of Figure 9(a) is multiplied by its matching-filter stored image of Figure 9(b). Figure 9(c) gives the product and Figure 9(d) the integral of the product as a function of time for $\tau = 0$. The autocorrelation function is shown in Figure 9(e). If the frequency is increased so that the signal has

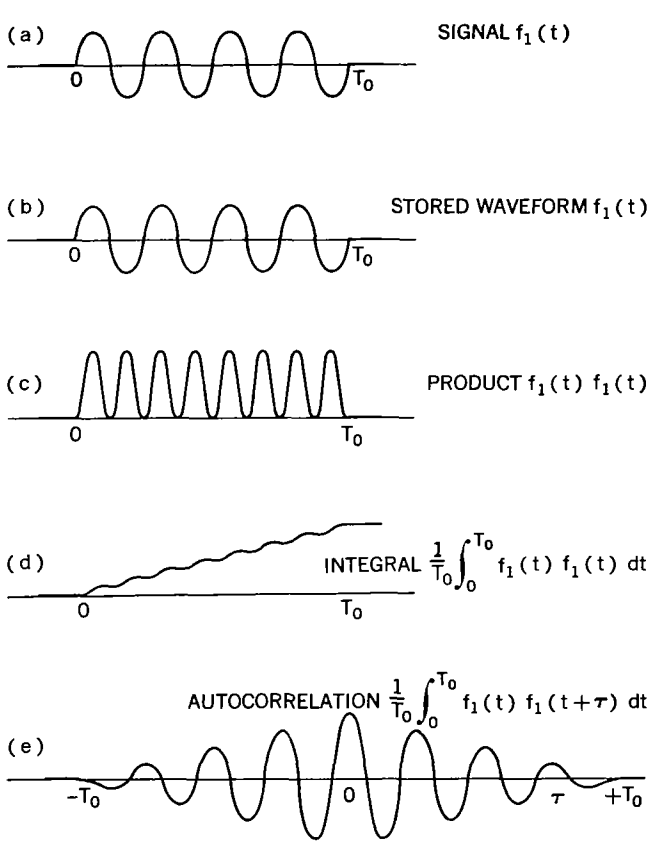

Figure 9—Matched-filter detection: (a) time-limited sine wave; (b) matching-filter stored image; (c) product; (d) autocorrelation function for $\tau = 0$; (e) autocorrelation function for values of τ.

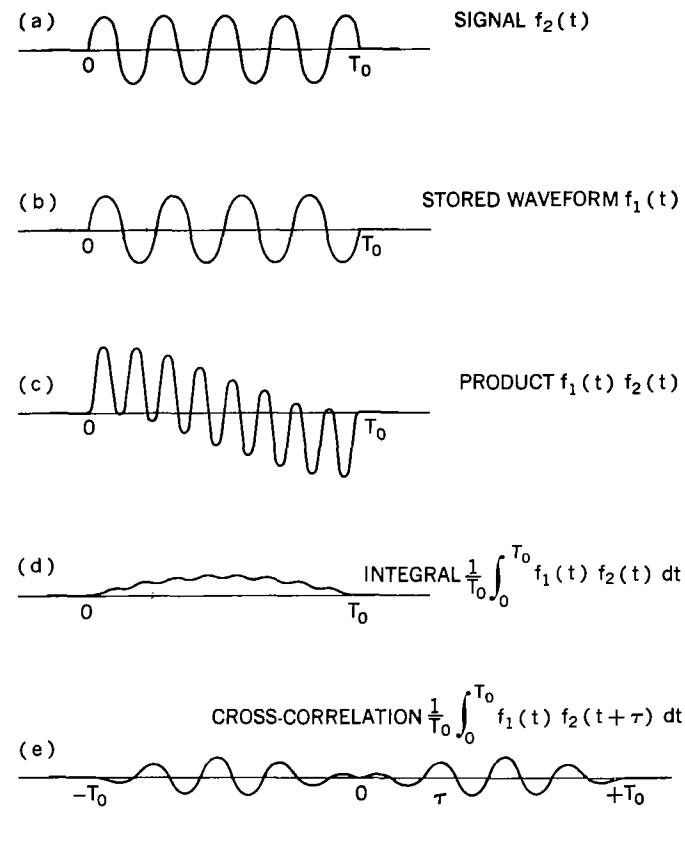

Figure 10—Matched-filter detection: (a) time-limited sine wave at higher frequency than stored image; (b) stored image; (c) product; (d) cross-correlation function for $\tau = 0$; (e) cross-correlation function for values of τ.

an extra half of a sine wave in the same pulse length T_0, then the signal is orthogonal to the filter, i.e., no match. Figure 10 shows the new signal of higher frequency, the correlating waveform (stored image in the filter), the product, the integral, and the general cross-correlation function.

Of interest is a plot of the cross-correlation function for $\tau = 0$ as a function of frequency:

$$\phi_{mn}(0) = \frac{1}{T_0}\int_0^{T_0} \sin\omega_m t\ \sin\omega_n t\ dt$$

$$= \frac{1}{2T_0}\left[\frac{\sin(\omega_m - \omega_n)t}{\omega_m - \omega_n} - \frac{\sin(\omega_m + \omega_n)t}{\omega_m + \omega_n}\right]_0^T$$

$$= \frac{\sin(\omega_m - \omega_n)T_0}{2(\omega_m - \omega_n)T_0} - \frac{\sin(\omega_m + \omega_n)T_0}{2(\omega_m + \omega_n)T_0} \quad . \tag{26}$$

The contribution of the second term will be small, so the covariance or cross-correlation for $\tau = 0$ is a $\sin x/x$ function. The eigenvalues of this function are obviously the allowed frequencies of the orthonormal set, since there is no cross-correlation at these points.

The eigenvalues occur when

$$\frac{1}{2}\,\frac{\sin(\omega_m - \omega_n)T_0}{(\omega_m - \omega_n)T_0} - \frac{1}{2}\,\frac{\sin(\omega_m + \omega_n)T_0}{(\omega_m + \omega_n)T_0} = 0 \,. \tag{27}$$

Both of these terms are zero if

$$(\omega_m - \omega_n)T = k\pi \quad \text{for } k = 1, 2, \cdots ,$$

and

$$(\omega_m + \omega_n)T = l\pi \quad \text{for } l = 1, 2, \cdots ,$$

Defining $\omega_n = \omega_m + \Delta\omega$ and substituting $\Delta\omega T_0 = k\pi$ and $(2\omega_m + \Delta\omega)\,T = l\pi$, we find that, if $k = 1$, then $\Delta\omega = \pi/T_0$ and

$$\Delta f = \frac{1}{2T_0} \,, \tag{28}$$

subject to the restriction that $\omega_m = l\pi/2T$.

The smallest allowable difference in frequency between any two members of a set of orthonormal frequencies is the reciprocal of twice the word length. It should be noted that the limit to the number of frequencies or eigenvalues that can be used in a set is usually dictated only by the limit on the complexity that can be tolerated.

Figure 11 is a plot of the cross-correlation function $\phi(0)$ as a function of ω_n for a fixed value of ω_m. The dashed curve is the amplitude spectrum of the pulsed sine wave. A practical example is a pulsed sine wave of 10 msec duration which has zeros of its cross-correlation with other frequencies in multiples of 50 cps; however, the zeros of the power spectrum of the pulsed sine wave fall in multiples of 100 cps away from the center frequency.

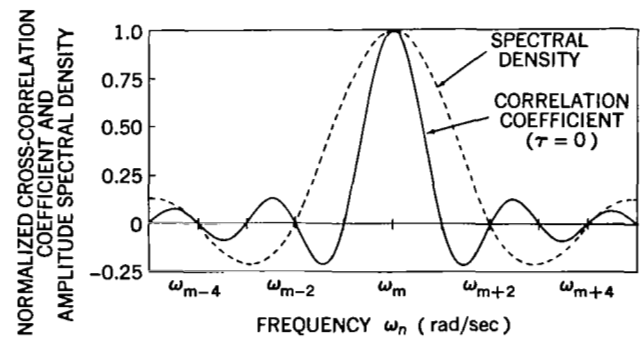

Figure 11—Cross-correlation function and power spectrum of pulsed sine wave $\left(f(t) = \sin(2\pi f_m t)\cdot\left\{u\left[t + (T_0/2)\right] - u\left[t - (T_0/2)\right]\right\}\right)$.

Amplitude spectral density curves for the general case when $f(t) = \sin(2\pi f_1 t + \theta)\cdot\left[u(t - \tau_1) - u(t - \tau_2)\right]$ are plotted in Figures 12 and 13. Figure 13 is varied in steps of

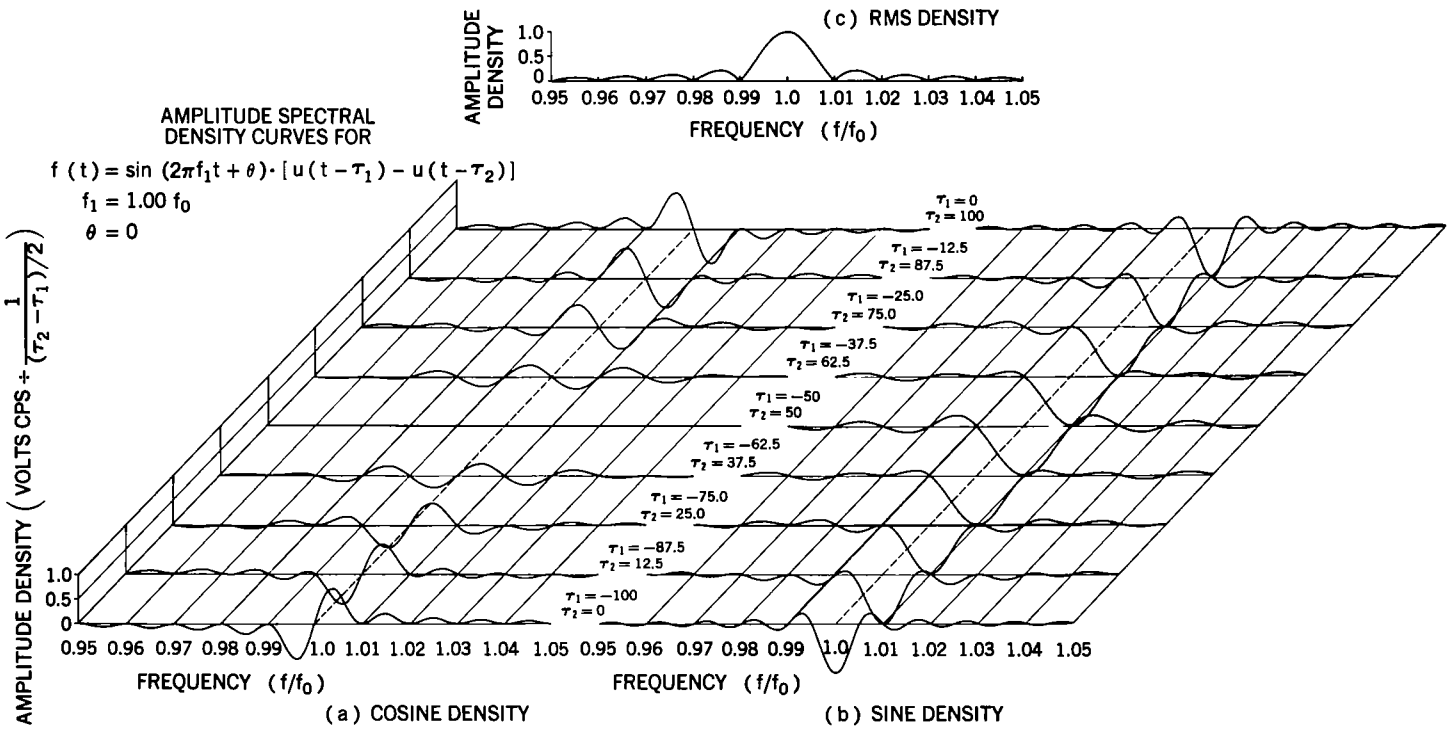

Figure 12–Amplitude spectral density curves for pulsed sine wave as a function of time shifting.

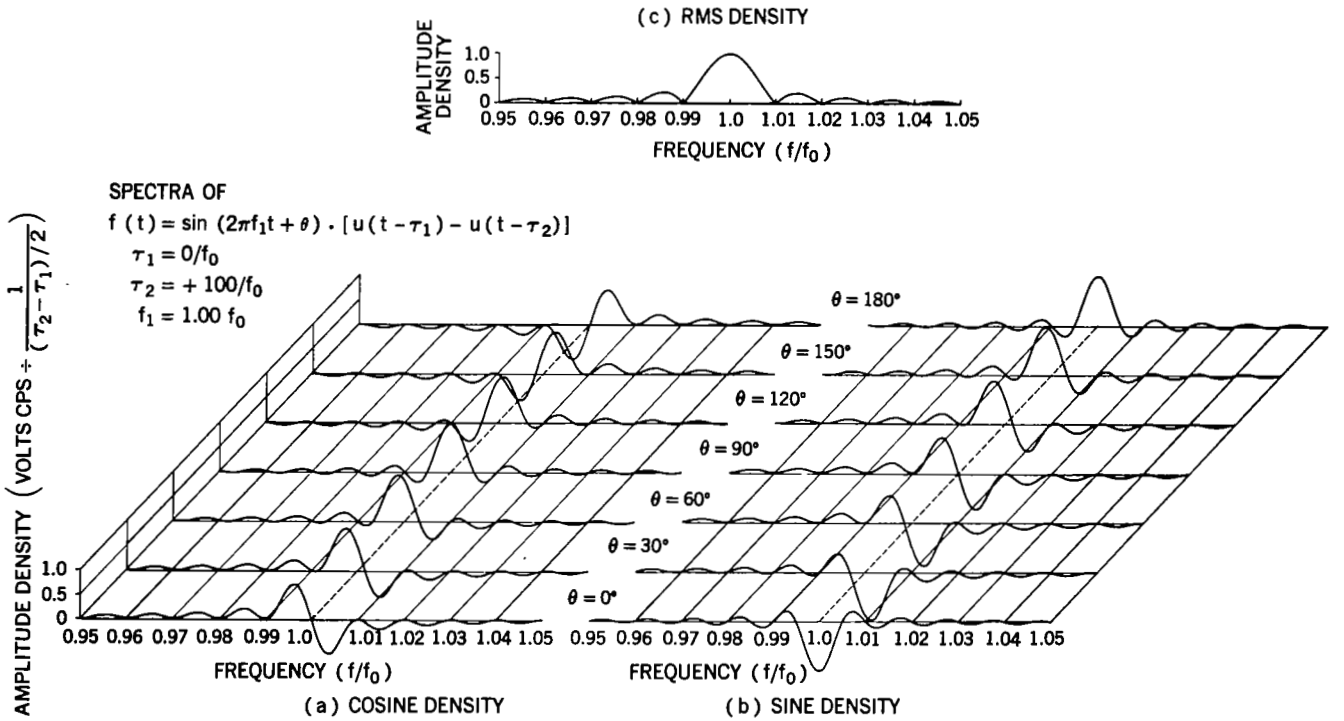

Figure 13–Amplitude spectral density curves for pulsed sine wave as a function of phase shifting.

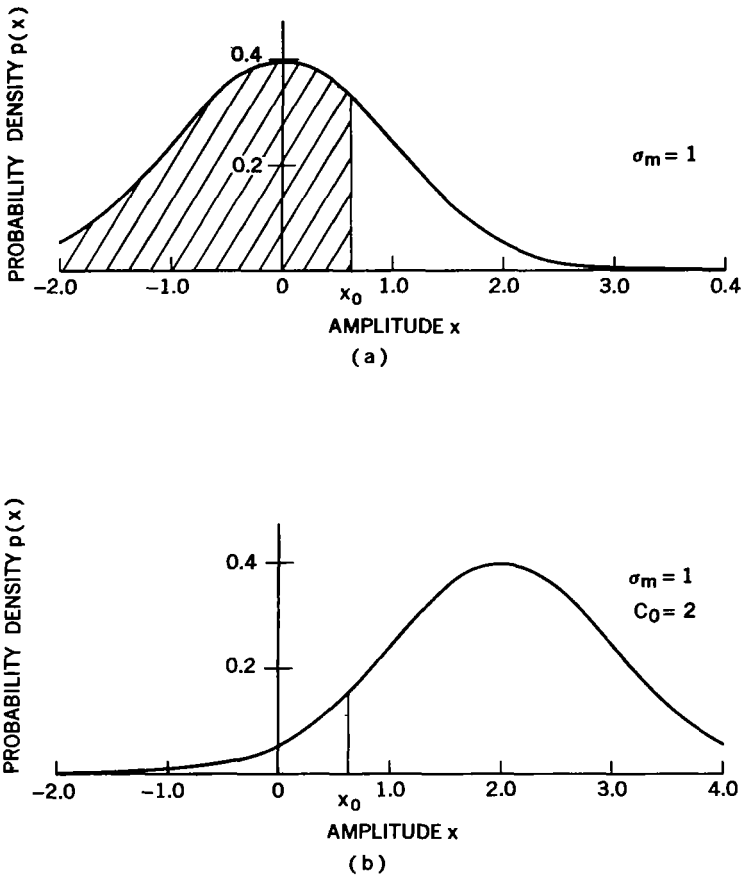

Figure 14—Probability density functions: (a) Gaussian noise; (b) signal plus Gaussian noise.

30 degrees for a total 180 degree change. The redistribution of densities can be seen.

Word-Error Probability for the Matched Filter

In calculating the word-error probability for the case of the the matched filters the same procedure is followed as for the unmatched filters, except that the character of the noise is changed. This noise has a Gaussian probability density [Figure 14(a)]. The probability density function for a signal of amplitude C_0 and noise is shown in Figure 14(b). The probability that there is no signal with an amplitude greater than x_0 in a filter is given by the integral of the Gaussian probability density function from $-\infty$ to x_0. Raising this probability distribution function to the N - 1 power gives the probability that is no signal greater than x_0 in any of the N - 1 filters. The probability that there is a signal at x_0 in the correct filter and that none of the other filters has an amplitude greater than x_0 is

$$p_c(N) = \left(\frac{1}{\sqrt{2\pi}\,\sigma_m} \int_{-\infty}^{x_0} e^{-x^2/2\sigma_m^2}\, dx \right)^{N-1} \frac{1}{\sqrt{2\pi}\,\sigma_m} e^{-(x_0 - C_0)^2/2\sigma_m^2}\, dx_0 \quad , \tag{29}$$

where σ_m^2 = variance of noise at output of matched filter, and C_0 = amplitude of signal at matched filter output. The probability of being correct for any amplitude x_0 is this integral over all values of x_0, from $-\infty$ to $+\infty$. The probability of an error is 1 minus the probability of being correct or

$$P_e(N) = 1 - \int_{-\infty}^{\infty} \left(\frac{1}{\sqrt{2\pi}\,\sigma_m} \int_{-\infty}^{x_0} e^{-x^2/2\sigma_m^2}\, dx \right)^{N-1} \frac{1}{\sqrt{2\pi}\,\sigma_m} e^{-(x_0 - C_0)^2/2\sigma_m^2}\, dx_0 \quad . \tag{30}$$

These curves have been programmed for computation on an IBM 7090 digital computer, and the results are plotted in Figure 15 for different values of n, the $\log_2$ of the number of filters used.

CONTIGUOUS-FILTER DETECTION SYSTEM

A set of contiguous filters with a maximum-likelihood detector can enhance the signal-to-noise ratio of a PFM-encoded signal. The maximum-likelihood detector samples all filters and decides

which filter contains the signal. This filter is connected to the output, so the signal-to-noise ratio is determined by the signal and noise in the one filter only. The output of the selected filter may be used in the following ways: (1) as an indicator that the signal was present; with N filters, 2^n levels of the signal can be detected, or the PFM word gives a precision of n bits; (2) to measure the frequency on the output of the selected filter in order to achieve a precision better than one part in 2^n. The latter technique may be applied only to an unmatched-filter set.

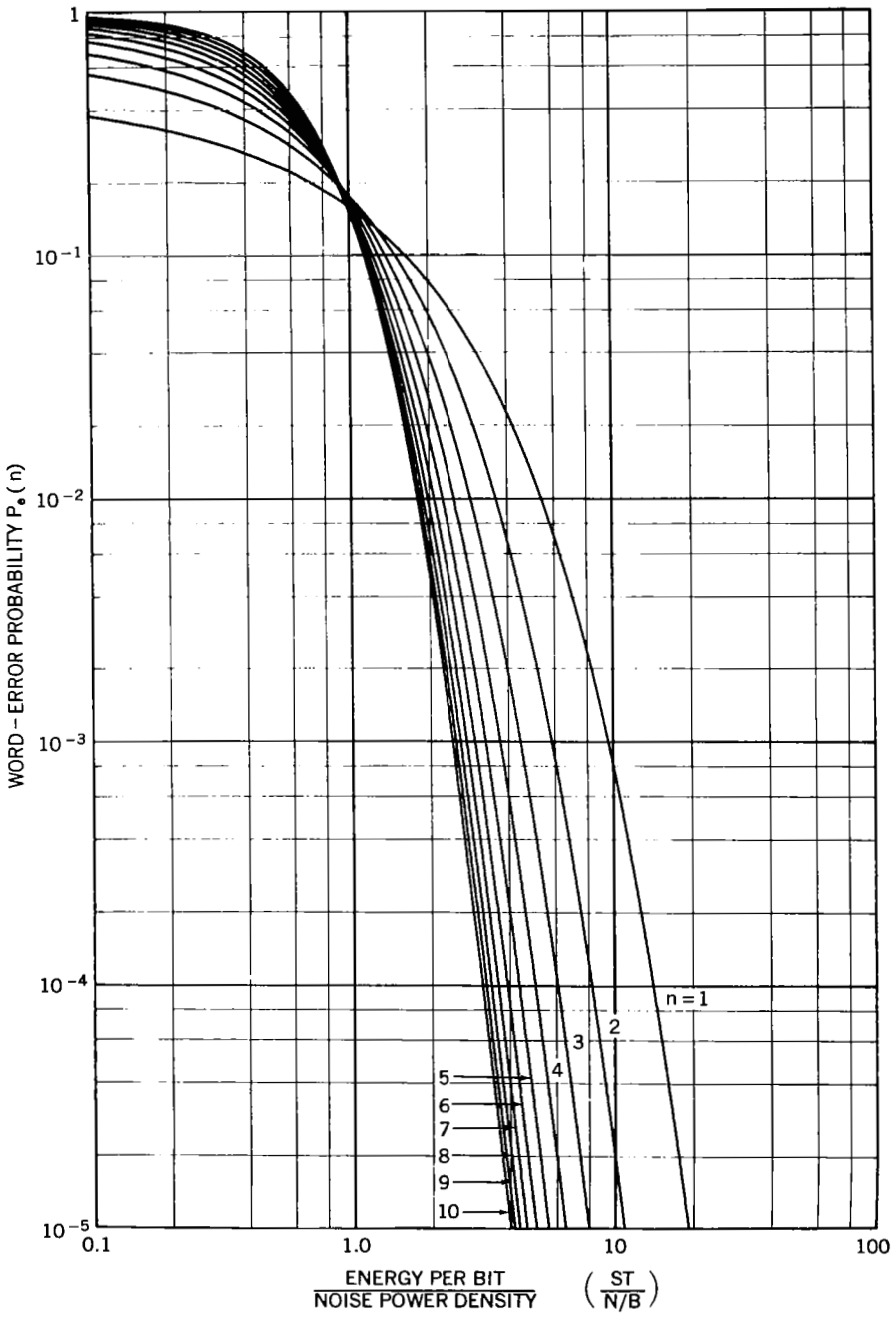

Figure 15—Word-error probability curves for Gaussian noise.

Analysis of Unmatched Filters

Earlier the noise analysis of a bandpass filter excited with random noise was given, and the error probability was calculated. It was assumed that the output of the filter contained no transients from the step input signal at the time of sampling, that the frequency of the input signal remained constant, and that an ideal filter was used. These assumptions will be considered in more detail now.

Response to Sinusoidal Step

The single-pole bandpass filter is the simplest and most economic filter that can be used to make a bank of contiguous filters. Consider the filter circuit in Figure 16. The transfer function is given by:

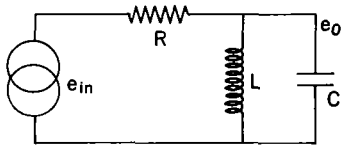

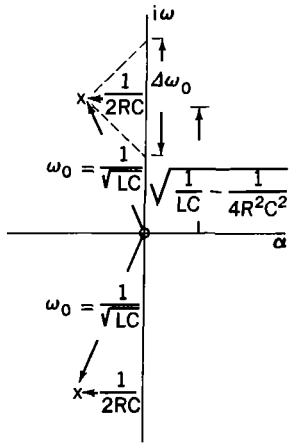

Figure 16–Filter element circuit.

$$\frac{E_0(s)}{E_{in}(s)} = \frac{\Delta\omega_0 s}{s^2 + \Delta\omega_0 s + \omega_0^2} , \qquad (31)$$

where $\Delta\omega_0 = 1/RC$ and $\omega_0 = 1/\sqrt{LC}$. The location of the singularities of the expression are plotted in Figure 16. We are interested in the output of the filter when the input is excited with a step sinusoid,

$$f(t) = C_1 \sin \omega_1 t \cdot u(t) . \qquad (32)$$

A convenient substitution is to let $\omega_0 = \omega_1 + \Delta\omega_1$ so that Equation 31 is a function of the excitation frequency and the difference between the excitation frequency and the resonant frequency of the filter. The equation for the response of a single-pole filter excited with a sinusoidal input of amplitude C_1 and frequency ω_1 is:

$$e_0(t) = \frac{\Delta\omega_0 C_1}{\left(\Delta\omega_0^2 + 4\Delta\omega_1^2\right)^{1/2}} \left(1 + e^{-\Delta\omega_0 t} - 2e^{-\Delta\omega_0 t/2} \cos \Delta\omega_1 t\right)^{1/2} \sin\left(\omega_1 t + \phi_2 + \phi_3\right) , \qquad (33)$$

where

$$\phi_2 = \tan^{-1} \frac{2\Delta\omega_1}{\Delta\omega_0} ,$$

$$\phi_3 = \tan^{-1} \left(\frac{e^{-\Delta\omega_0 t/2} \sin \Delta\omega_1 t}{e^{-\Delta\omega_0 t/2} \cos \Delta\omega_1 t - 1} \right) .$$

Equation 33 is derived in Appendix C.

It is instructive to examine the terms of this equation for transient effects during a frequency measurement. One method of frequency measurement is to determine the period of each cycle and find a k period average. The averaging is started at least 1 time constant, $1/\Delta\omega_0$ seconds, away from the leading edge of the pulse and may be continued until the end of the pulse. The value ϕ_2 will have no effect upon the measurement since it represents a constant phase shift of the zero crossings; however, ϕ_3 definitely contributes to the frequency measurement error if $e^{-\Delta\omega_0 t/2}$ is not damped appreciably. Figure 17 is a plot of $\phi_2 + \phi_3$ against time, for values of $\Delta\omega_1$ ranging from the frequency of the center of the adjacent filter to the frequency of the center of the filter under investigation. From these curves and the start and stop times for the frequency measurement, the error in frequency can be calculated (Figure 18).

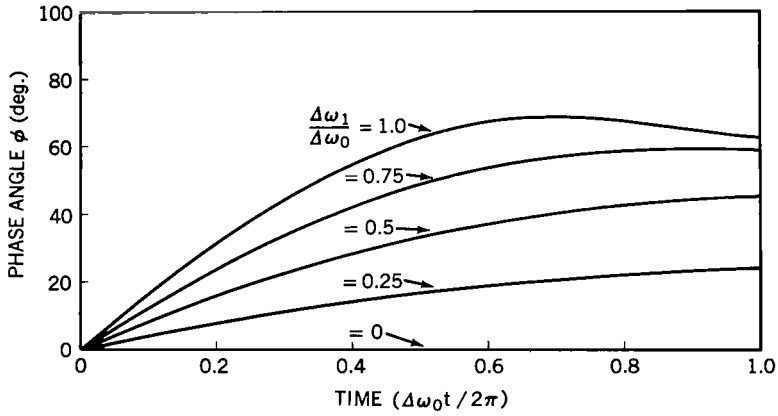

Figure 17—Phase response to step sinusoid for a single-pole filter.

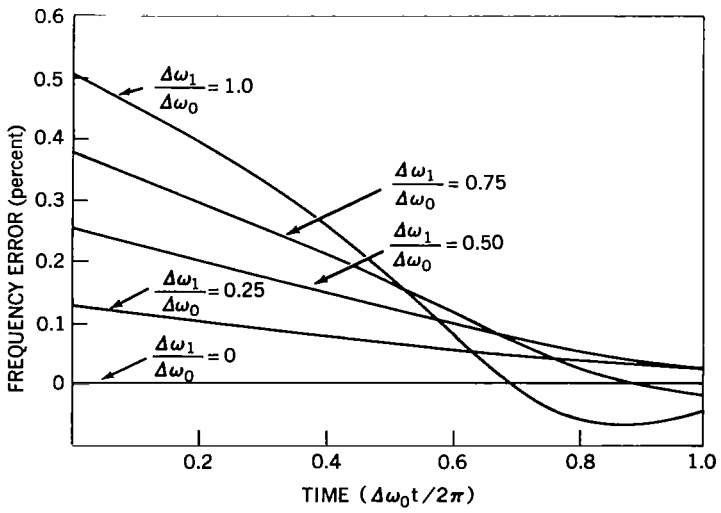

Figure 18—Frequency error from response of a single-pole filter to a step sinusoid.

Response to a Gliding Tone

The case for the PFM excitation frequency not centered in the filter has been examined. Of considerable interest is the case for the signal which is changing frequency while it is in the filter. This frequency change is very evident when sample-and-hold techniques are not used in the analog oscillators. A spin-stabilized spacecraft can frequency modulate any vector-type measurement at the spin frequency.

The solution for the continuous gliding tone has been given by Barber and Ursell (Reference 17). In Appendix D the equation for a step-function changing frequency is derived. The convolution of the excitation function with the impulsive response of the single-pole filter is

$$h(t) = \Delta\omega_0 A_I e^{-\Delta\omega_0 t/2} \left[\cos\left(\omega_0 t + \tan^{-1}\frac{\Delta\omega_0}{2\omega_0}\right) \cdot \right.$$

$$\cdot \int_0^t e^{\Delta\omega_0 \tau/2} \cos\omega_0\tau \cdot \sin\left(\omega_1 \tau - \frac{\omega_d}{\omega_a}\cos\omega_a\tau\right) d\tau$$

$$\left. + \sin\left(\omega_0 t + \tan^{-1}\frac{\Delta\omega_0}{2\omega_0}\right) \cdot \int_0^t e^{\Delta\omega_0\tau/2} \sin\omega_0\tau \cdot \sin\left(\omega_1\tau - \frac{\omega_d}{\omega_a}\cos\omega_a\tau\right) d\tau \right], \quad (34)$$

where ω_a is the peak frequency deviation and ω_d is the modulation frequency.

If the rate of change of frequency is too great, the filter does not have sufficient time to respond, and the output is attenuated. Equation 34 has been programmed on an IBM 7090 computer to determine the attenuation for various rates of frequency change. The parameters for the Explorer X space probe telemeter were used to compute an amplitude-frequency-time plot. A three-dimensional model was constructed to show the interesting results of the beating of the transient response and the gliding excitation function; a photograph of the model is shown in Figure 19. In this figure time is the x-axis coordinate, and the scale along the x-axis depicts half of a revolution of the spacecraft. The y-axis is in units of the center frequency of a filter $\Delta\omega_0$ radians per second in width. The z-axis is the amplitude of the envelope of the output of a filter. Parameters for Explorer X used in the calculation were: a bandwidth of 25 cps for a filter, 100 filters covering the frequency range from 1.75 to 4.25 kc; and a sinusoidal varying frequency centered at 3 kc, with a maximum deviation of 1 kc for a spin frequency $\omega_s/2\pi$ of 1.8 cps. The responses of 17 filters distributed between 3 and 4 kc were calculated and plotted. These were used as templates in the construction of the model. Any cross-section parallel to the time axis gives the response of the filter of that frequency to the gliding tone (Figure 20).

Matched-Filter Techniques

Matched filters used with a maximum-likelihood-detector system provide the optimum in signal detection. These techniques can be applied to PFM-encoded signals if phase coherence is maintained at the beginning of each pulse.

It can be noted in Figure 10 that the signal and stored image are phase coherent at the beginning of the pulse. For perfect orthogonality, only those frequencies of the signal are allowed which cause an integral number of half cycles in the pulse. Since the phase of analog PFM signals can have any value and the signals are therefore not always orthogonal, it is not possible to use the matched-filter techniques directly. A compromise which allows the use of these techniques is to force the phase of

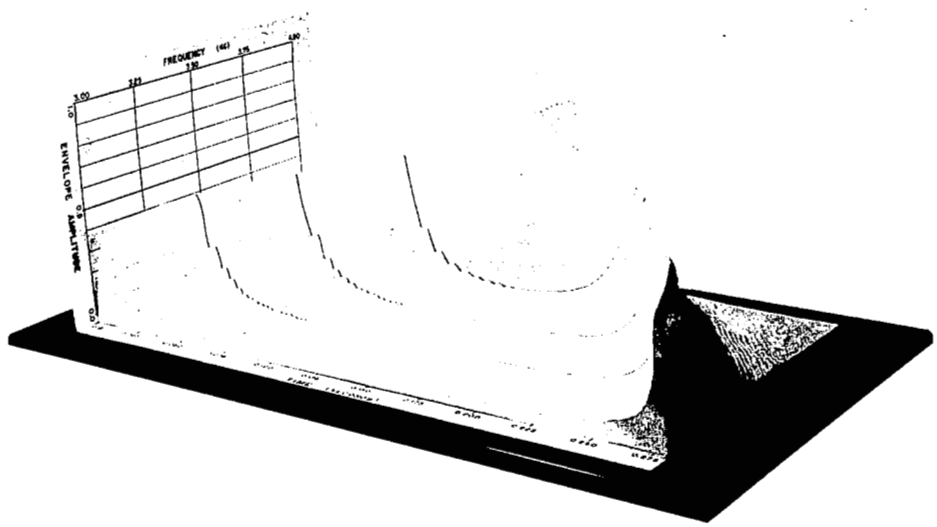

Figure 19—Amplitude-frequency-time function of the response of a single-pole filter to a gliding tone.

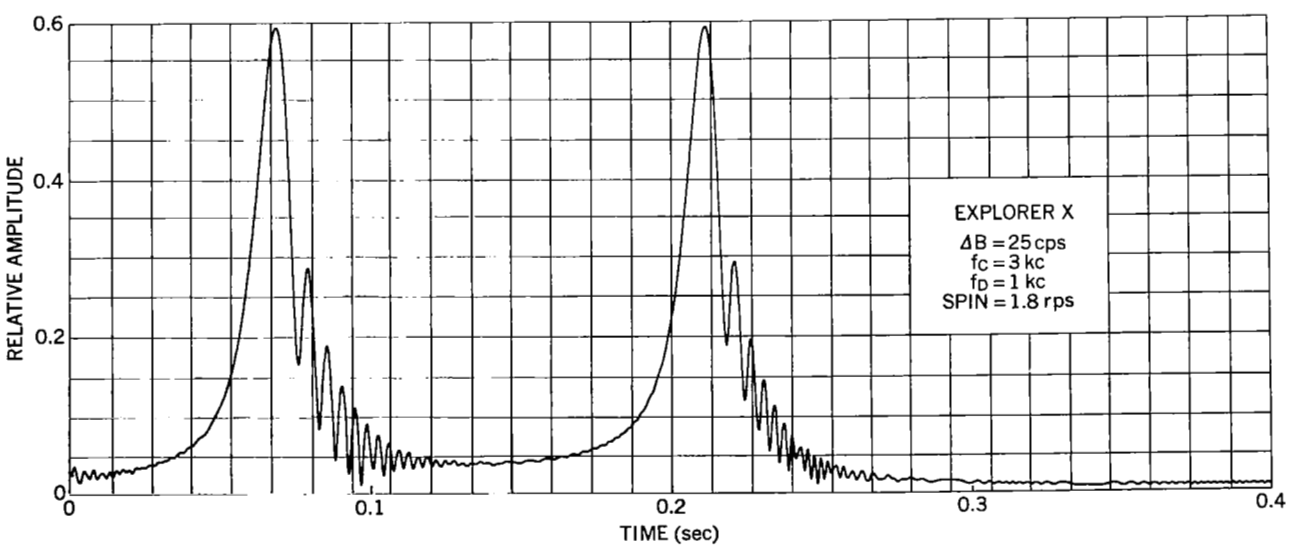

Figure 20—Response of one single-pole filter to a gliding tone.

the pulsed subcarrier oscillator to start always in the same phase at *a priori* known times. The phase at the end of the pulse is, of course, unknown. But, if the frequency separation of the stored image is governed by the relation $\Delta\omega = \pi/T_0$ (Equation 28), where $\Delta\omega$ is the angular frequency separation and T_0 is the length of the pulse, then the correlation coefficient for one of the N correlators will always be at least $1/\sqrt{2}$ of the maximum. However, when this occurs, it will occur in two correlators simultaneously. This area has not, as yet, been investigated thoroughly, but the technique should be applicable to the telemetry signals received from Ariel I. A tape recorder aboard the satellite played back signals of stored PFM analog and digital oscillator pulses. Because of the ratio of record to playback speeds, the frequencies of the oscillators were scaled down by a factor of 48 to 1. This forced each pulse to start in the same phase and should allow application of the matched-filter technique to data already received.

EXPERIMENTAL RESULTS

Spectral Analysis

The operation of a set of contiguous filters combined with a maximum-likelihood detector can become quite complicated, especially when the signal is derived from magnetic tape recordings of actual satellite passes. Since output is influenced by many variables, evaluation in conditions of poor signal-to-noise ratios is difficult. To obtain a more qualitative estimate of the value of the contiguous-filter system, an experimental system was set up so that measurements under actual noisy conditions could be made.

The equipment consisted of a tape scanner which performs the same task as an endless loop tape recorder. The tape scanner has a seven-track reproducing head mounted on a revolving 1-foot-diameter disk. The tape is in contact with half of the circumference of the disk so that, with the tape motionless and the disk rotating, the head sweeps along the tape for half of each revolution of the disk. The peripheral speed of the disk is 30 ips. Thus, it is possible to scan one portion of a magnetic tape recording many times and observe the output on an oscilloscope.

By inserting a wave analyzer between the tape scanner and the oscilloscope, the spectral content of the signal for any pulse duration T and bandwidth $\Delta\omega_0$ can be obtained. A Quan-Tech Model 303 Wave and Noise Spectrum Analyzer set at a bandwidth of 100 cps was used to obtain the envelope of the signal and noise in the 100 cps bandwidth over the frequency range of 3.6 to 16.4 kc. An important advantage of the Model 303 Analyzer is the flat-topped filter characteristic, which is a Butterworth approximation. It provides, for this purpose, a good approximation to an ideal filter.

By very slowly changing the center frequency of the analyzer as a section of tape is scanned, a spectral analysis of the signal can be made. The output of the analyzer is used to intensity-modulate the beam of the oscilloscope as the sweep is being triggered at the beginning of each revolution of the scanner. The analyzer has a dc output which is proportional to the position of the frequency dial; this voltage is used on the y-axis of the oscilloscope in the same manner as the vertical deflection on a television raster. By taking a time exposure of the oscilloscope face, a high quality spectral

analysis of the signal is produced. The x-axis represents time, the y-axis is a function of the frequency, and the intensity represents the energy in a filter at a particular time.

An interesting aspect to the problem developed as this equipment was being checked. Explorer XII, the Energetic Particles Satellite, suddenly ceased transmitting after approximately 2000 hours of continuous operation. The signal was last heard over Woomera, Australia, at a range of 65,000 km. It was highly desirable to examine the magnetic tape recordings at the time of failure to see if any clues could be obtained on the possible cause of failure. Some of the equipment aboard Explorer XII was identical to that to be used in the next scheduled spacecraft so that, if the trouble area were located, corrective measures could be taken before flight.

A copy of the Woomera tape was played on the tape scanner into the wave analyzer. Close examination of the output at the point where the signal apparently disappeared revealed that the signal was still present although attenuated by about 10 to 15 db. The signal remained at this level for 2 seconds and then disappeared completely. During these last 2 seconds, seven frames of the telemetry were received. Although the signal-to-noise ratio was poor during this interval, the majority of the channels could be read. The tracking filter used at the ground station was swinging in and out of lock because of the large amount of noise in the feedback loop. This caused a random obliteration of some channels.

To demonstrate the noise-immunity characteristics of PFM, the complete failure sequence is shown in Figure 21. Two spectral analysis photographs were taken of each telemetry frame; one covered the frequency range from 4.5 to 10 kc and the other from 10.0 to 18.0 kc. Composite photographs were then made up from the twelve photographs of each six frames. A set of these cover the time span from fourteen frames before the signal disappearance to nineteen frames afterward. In order to maintain high resolution along the frequency axis, the frequency dial was motor driven at a rate sufficient to yield at least 300 horizontal lines per photograph; this gives an effective 600 lines in the vertical dimension.

The failure sequence started between the ninth and the tenth channel pulses in telemetry frame zero. The increase in noise is immediately apparent since the tracking filter at the ground receiving station increased its gain to compensate for the loss in signal; however, evidence of signal energy in channels one through six is very definite in telemetry frame one. Because of the redundant nature of some of the data, the frequencies of these channels could be predicted a few frames in advance. With this *a priori* information, it was easy to establish the existence of the signal for the 2-second period after the signal disappeared. During this time all channels appeared to be giving their normal indications. This cleared the majority of the spacecraft subsystems from suspect and left only the transmitter and transmitter power converter to be investigated further.

The instantaneous decrease in output power of approximately 15 db could be attributed to either a failure in the transmitter output stage or a loss of power from the transmitter converter. There was enough interelectrode capacitance in the transmitting tube to allow a feed-through of energy from the transmitter oscillator-buffer stage to the antenna. Because of the catastrophic failure at the end of the 2-second attenuation period, it is probable that the failure occurred in the transmitter

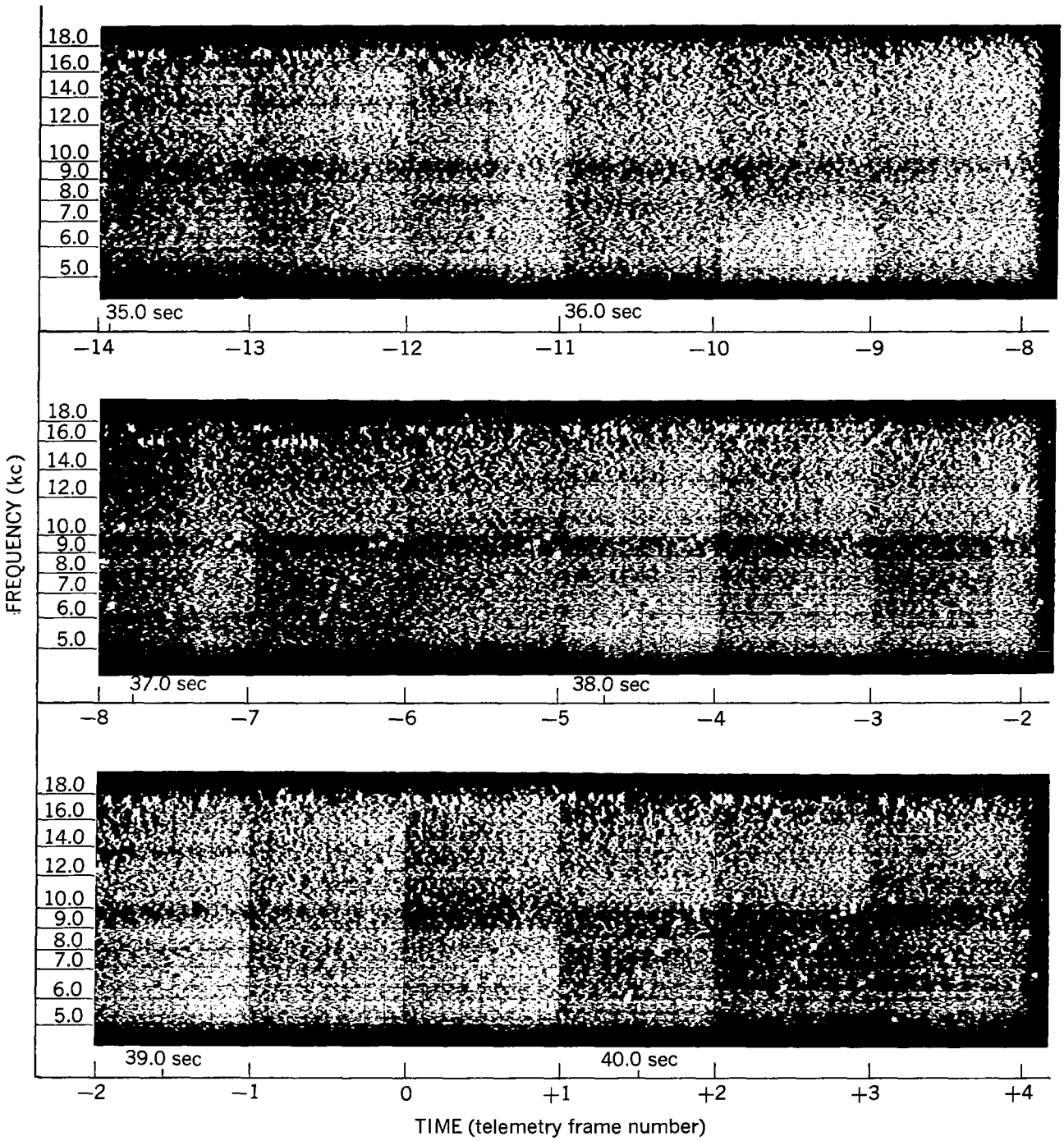

Figure 21—Spectral analysis of PFM telemetry signals.

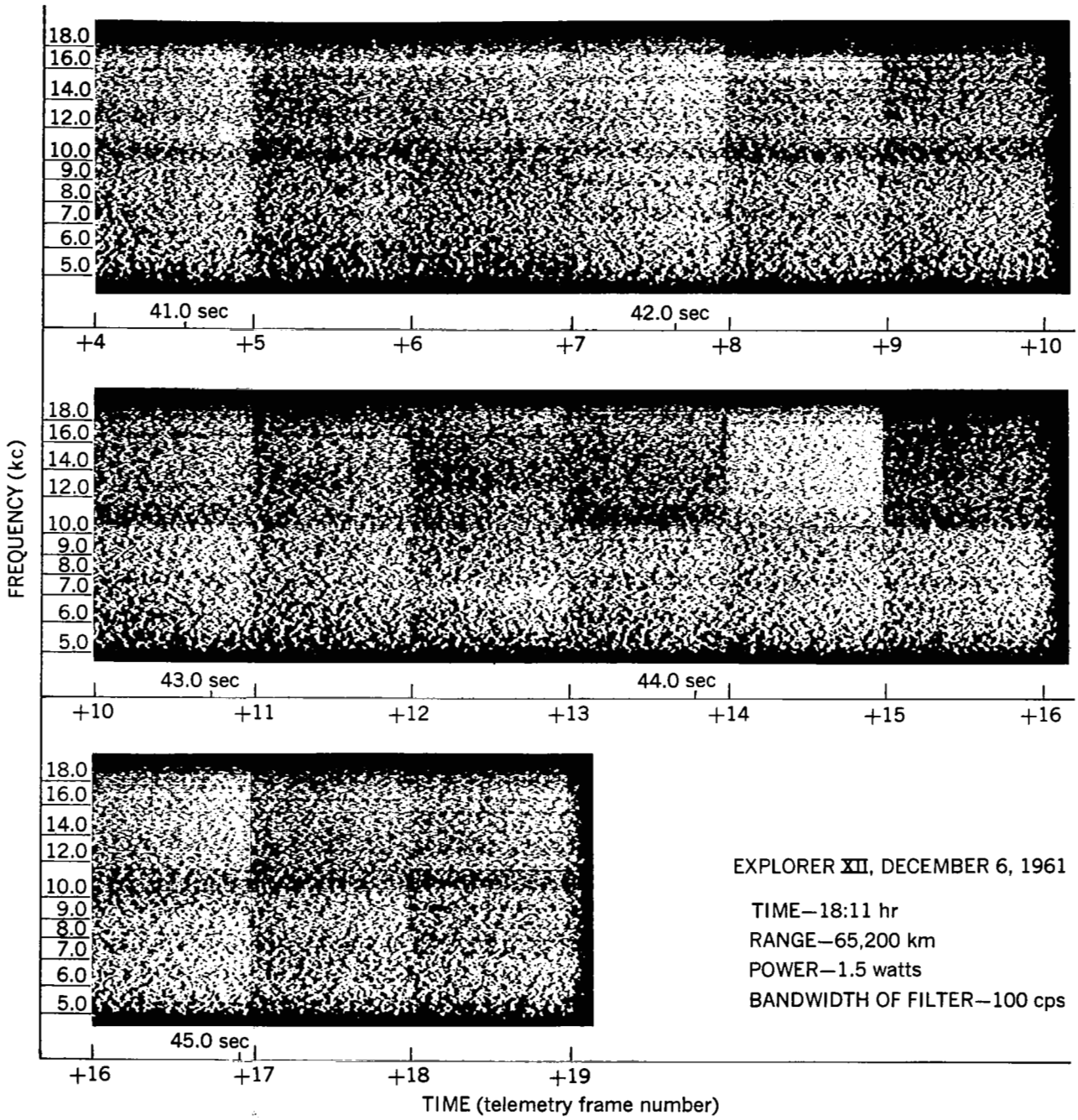

Figure 21—Spectral analysis of PFM telemetry signals. (cont.)

converter. Subsequent flights were scheduled to use all-transistorized transmitters; therefore the potential trouble sources would be eliminated.

This method of spectral analysis is not extremely effective for presenting noisy data. The number of intensity levels that the human eye can distinguish is fairly limited. To aid in increasing the contrast between signal and noise, the output of the wave analyzer was passed through an RC network which added a small amount of the derivative of the input to its output. The objective was to give the picture more of a three-dimensional look by casting "shadows" on one side of each PFM pulse. The effect is very prominent on the original photographs, although some of the effect is lost in the reproduction of these figures. The block diagram of the equipment used in making the photographs is shown in Figure 22, which also includes the circuit diagram of the network giving the three-dimensional effect.

This same technique of spectral analysis was applied to the recording of the amplitude modulation output of the tracking filter; the results are shown in Figure 23. Before the failure there was a strong 50 cps component, the phase of which was used to provide channel synchronization. The third and fifth harmonics of this frequency can also be seen. The series of impusles spaced slightly less than 1 second apart are a result of the shadowing of the solar cells by their supporting paddles. This introduced a transient into the power system and caused a slight pulling of the transmitter frequency. At 39.75 seconds the intensity decreases; the signal completely disappears at 41.8 seconds. These composite photographs were taken without the RC network since only continuous signals were being observed.

Signal-to-Noise-Ratio Comparisons

The Woomera tape provided an excellent opportunity to compare theoretical calculations of the signal-to-noise ratio and the error probability with actual measurements. The calculations are made as follows:

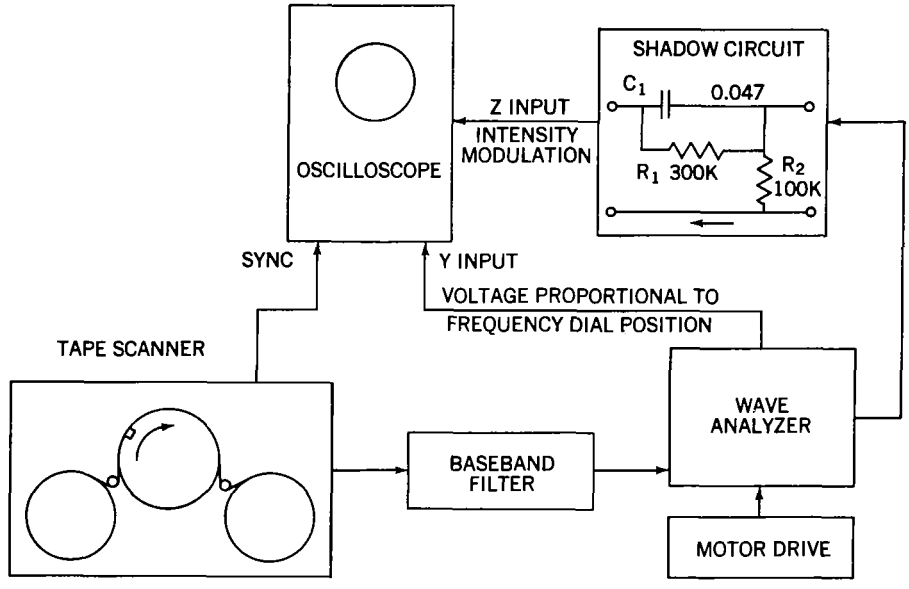

Figure 22—Block diagram of spectral analysis equipment.

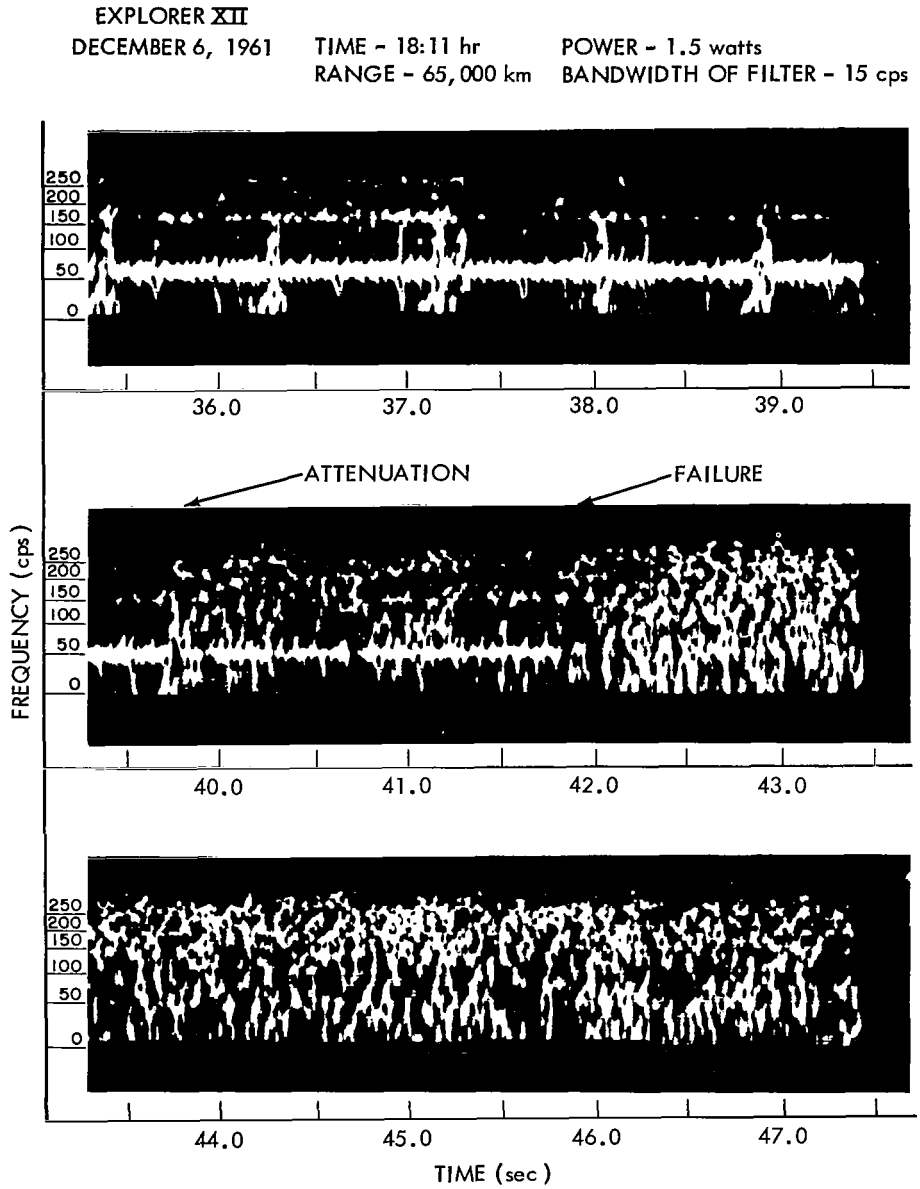

Figure 23–Spectral analysis of telemetry receiver AM output during failure sequence.

1. *Determine the received signal power:*

The measured prelaunch transmitter power was 1.5 watts. The sideband power for a ±57 degree phase-modulated signal is twice the carrier power or 1.0 watt (P_t = +30.0 dbm) . The transmitting antenna gain includes the dipole gain, wiring harness loss, and circular polarization loss (G_t = -4 db) . The receiving antenna gain is taken from quoted values of gain for an array of 16 crossed-yagi antennas (G_r = +21 db) . Attenuation due to the 63,200 km path loss is

$$\left(\frac{\lambda}{4\pi r}\right)^2 = \left(\frac{300}{136 \times 4\pi \times 63.2 \times 10^6}\right)^2$$

$$= -171.1 \text{ db} .$$

Substitution of these factors in the received power equation yields:

$$W_r = P_t G_t G_r \left(\frac{\lambda}{4\pi r}\right)^2$$

$$= +30.0 - 4 + 21 - 171.1$$

$$= -124.5 \text{ dbm} .$$

2. *Determine the received noise power*

The galactic noise temperature (Reference 18) at 136 Mc in the plane of the ecliptic has an average value of about 600°K; however, there is a hot spot of about 2000°K looking toward the center of the galaxy. The receiver noise temperature is quoted at 3 db. This corresponds to a receiver noise temperature of 290°K. The noise temperature due to the earth and atmospheric noise as sensed by the antenna side lobes is 55°K. Since synchronous detection was performed on the carrier by the station tracking filters, the noise bandwidth can be taken to be the width of the individual filter in the contiguous-filter bank employed in data reduction. This bandwidth is 100 cps. Therefore the received noise power is

$$P_n = kTB \text{ watts}$$

$$= 1.38 \times 10^{-23} \times 945 \times 100$$

$$= 1.305 \times 10^{-15} \text{ mw}$$

$$= 148.9 \text{ dbm} ,$$

where

$k = 1.38 \times 10^{-23}$ watt-sec/deg,

$T = 600° + 290° + 55° \approx 945°K$,

$B = 100$ cps .

3. *Determine the signal-to-noise ratio*

The calculated signal-to-noise ratio is

$$\frac{W_r}{P_n} \approx -124.5 - (-148.9)$$

$$= 24.4 \text{ db} .$$

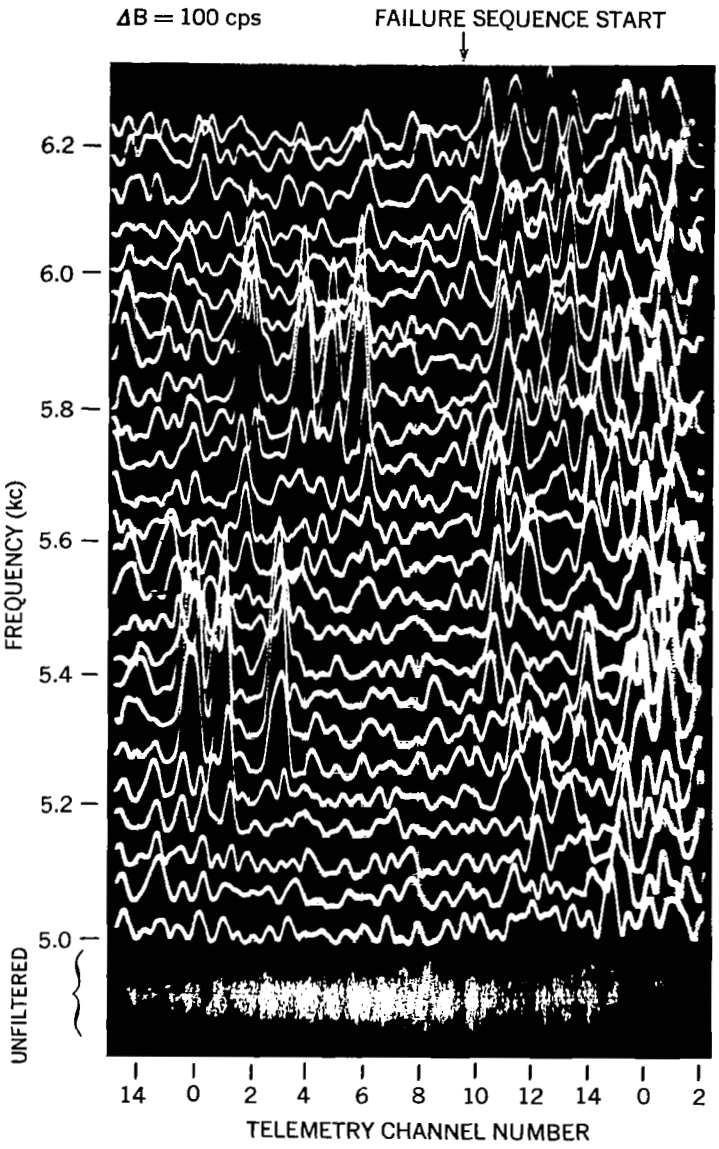

Figure 24—Spectral analysis of telemetry frame of Explorer XII at time of failure.

A reasonably accurate signal-to-noise-ratio measurement can be taken from Figure 24. The x-axis encompasses one telemetry frame, and each trace in the y direction represents a change of 50 cps in the filter center frequency. The signal amplitude can be measured fairly accurately, but a good qualitative measurement of the noise is more difficult. The voltage signal-to-noise ratio is estimated to fall between 10 and 15 to 1 or between 20 and 23.5 db. This compares very favorably with the calculated value of 24 db; however, it should not be too close, since we have calculated the input signal-to-noise ratio and assumed that it is the same as the output ratio. But the actual measurement is, on the other hand, purely the output signal-to-noise ratio.

A more meaningful measurement is the word-error probability. An examination of the data print-out records taken on a typical operational data-reduction line, which uses a bank of contiguous filters, indicated that the word-error probability just prior to the failure sequence was 10^{-2}.

If the word-error probability curves for Rayleigh noise of Figure 8 are used, the error probability for 24 db, after adjustment for the number of bits in the word and by using the total variance, is still greater than 10^{-5}. The operational contiguous filters have a threshold detector which must be exceeded before data are printed out. The actual errors in the operational data reflect the effects of the threshold detector and are not representative of theoretical filters operating with maximum-likelihood detectors.

CONCLUSION

The object of this report has been twofold: to present some of the characteristics of pulse-frequency modulation; and to show that pulse-frequency modulation, with certain restrictions, is a special PCM group code of coded binary sequences having orthonormal characteristics.

A number of successful spacecraft have used pulse-frequency modulation as the encoding technique. In the decoding of their analog data, a set of contiguous filters was used to extract the magnitude of the original signal. Since the individual filters were not flat within their passbands, degradation of the signal-to-noise ratio occurred if the encoded signal did not fall exactly in the center of a filter. Also, for response-time considerations, the filter bandwidth was equated to the reciprocal of the pulse length. By employing cross-correlation techniques using maximum-likelihood detectors, the resolution of the measurement can be doubled for the same pulse length without increasing the baseband width. This emphasizes an outstanding characteristic of pulse-frequency modulation: Quantizing errors for analog signals are not forced into the data at the source; the quantization is accomplished during the reduction of the data. The signals are encoded in a manner which approaches the maximum communication efficiency; the amount of enhancement of the signal-to-noise ratio depends on the sophistication of the decoding process.

The method of presenting the cross-correlation coefficients (when $\tau = 0$) of binary sequences in a matrix array aids in visualizing the communication efficiency that can be expected for any particular grouping of the sequences. The method ties together the efficiency of group and parity codes, and the same techniques can be applied to other codes, such as the Bose-Chaudhuri code, which have more members per set but are less efficient (Reference 19). The correlation tables for any of these coding schemes can be generated conveniently by means of a digital computer.

Error-probability curves have been derived for the unmatched-filter set, with maximum-likelihood detection, perturbed by Rayleigh noise. The matched-filter case has also been given so that direct comparisons may be made. With large signal-to-noise ratios, the probability of a word error as given by the Rayleigh probability density function approaches the error probability for the matched filter given by the normal probability density function. At lower signal-to-noise ratios, the matched filter is appreciably better than the unmatched; however, at these low values, the high error probability usually renders the data useless.

The output of a single-pole bandpass filter in a set of contiguous unmatched filters, can be fed into a discriminator to determine the frequency more accurately. The transient terms generated by the excitation of the filter with a step-function sinusoid introduce a small error in the frequency measurement of the pulse. The error is a function of the displacement of the pulse frequency from the center frequency of the filter, although its magnitude may be neglected in most cases.

Calculations were presented for the response of a single-pole filter to a sinusoidally varying frequency. The beating of the transient response of the filter with the excitation frequency was illustrated in the model of the amplitude-frequency-time relation with parameters for a typical spacecraft.

Nothing has been said about the methods of implementation of the encoding process. These methods are now fairly well established as practical engineering techniques. Instead, the emphasis has been on the versatility of pulse-frequency modulation as an encoding technique. It is hoped that this work will stimulate effort to provide as much versatility in signal decoding as now exists in the encoding process.

ACKNOWLEDGMENTS

It is with sincere appreciation that I acknowledge the contributions of my associates at Goddard Space Flight Center who have aided in the successful application of pulse-frequency modulation to satellite communication. I would like to thank Mr. P. T. Cole, who designed and developed the tape scanner used to extract signals buried in noise. I would also like to mention Mr. David H. Schaefer for his efforts on the digital pulsed subcarrier oscillator; Mr. Roland L. Van Allen for his original work on the analog pulsed subcarrier oscillator; and Mr. Clarence B. House for his work on special devices which enhance the applicability of PFM; Mr. J. H. Perry for his very careful efforts in the layout and construction of the first printed circuit modules for the Vanguard III Satellite; Mr. Hosea D. White for his tireless effort in reducing PFM circuitry ideas to practical application; and Mr. Curtis M. Stout for his outstanding contributions to the solution of PFM data-reduction problems. I am also grateful to Dr. Norman F. Ness who introduced me to the concept of the large scale digital computer as an everyday engineering tool.

REFERENCES

1. Shannon, C. E., "A Mathematical Theory of Communication," *Bell System Tech. J.* 27(3):379-423, July 1948; 27(4):623-656, October 1948.
2. Kotel'nikov, V. A., "The Theory of Optimum Noise Immunity," New York: McGraw-Hill, 1959, pp. 46-48.
3. Carson, J. R., "Notes on the Theory of Modulation," *Proc. IRE* 10(1):57-64, February 1922.
4. Armstrong, E. H., "A Method of Reducing Disturbances in Radio Signaling by a System of Frequency Modulation," *Proc. IRE* 24(5):689-740, May 1936.
5. Goodall, W. M., "Telephony by Pulse Code Modulation," *Bell System Tech. J.* 26(3):395-409, July 1947.
6. Hamming, R. W., "Error Detecting and Error Correcting Codes," *Bell System Tech. J.* 29(2):147-160, April 1950.
7. Viterbi, A. J., "On Coded Phase-Coherent Communications," *IRE Trans. on Space Electronics and Telemetry* SET-7(1):3-14, March 1961.
8. Rochelle, R. W., "Earth Satellite Telemetry Coding System," *Elect. Eng.* 76(12):1062-1065, December 1957.
9. Linden, D. A., and Abramson, N. M., "A Generalization of the Sampling Theorem," *Info. and Control* 3(1):26-31, March 1960.
10. Reed, I. S., "A Class of Multiple-Error-Correcting Codes and the Decoding Scheme," *Trans. IRE Prof. Group on Information Theory* PGIT-4:38-49, September 1954.
11. Sanders, R. W., "Digilock Telemetry System," in: *Proc. Nat. Sympos. on Space Electronics and Telemetry, San Francisco, September 1959,* New York: IRE Prof. Group on Space Electronics and Telemetry, 1959, Paper 6.3.

12. North, D. O., "An Analysis of the Factors Which Determine Signal/Noise Discrimination in Pulsed Carrier Systems," Radio Corp. Amer. Lab. Rept. PTR-6C, June 25, 1943.

13. Helstrom, C. W., "Statistical Theory of Signal Detection," New York: Pergamon Press, 1960, pp. 91-95.

14. Campbell, G. A., and Foster, R. M., "Fourier Integrals for Practical Applications," Princeton, N. J.: Van Nostrand, 1948.

15. Rice, S. O., "Mathematical Analysis of Random Noise," *Bell System Tech. J.* 23(3):282-332, July 1944; 24(1):46-156, January 1945.

16. Wainstein, L. A., and Zubakov, V. D., "Extraction of Signals from Noise," Englewood Cliffs, N.J.: Prentice-Hall, 1962, pp. 86-91.

17. Barber, N. F., and Ursell, F., "The Response of a Resonant System to a Gliding Tone," *Phil. Mag.* 39(292):345-361, May 1948.

18. Ko, H. C., "The Distribution of Cosmic Radio Background Radiation," *Proc. IRE* 46(1):208-215, January 1958.

19. Bose, R. C., and Ray-Chaudhuri, D. K., "On a Class of Error Correcting Binary Group Codes," *Info. and Control* 3(1):68-79, March 1960.

Appendix A

Amplitude Density Spectrum of a Pulsed Sine Wave

Let $f(t)$ be a pulsed nonrecurring sine wave of frequency ω_1, phase angle θ, and pulse length $\tau_2 - \tau_1$ (Figure A1). From the Fourier transform of $f(t)$ the amplitude density spectrum of a pulsed sine wave is

$$F(\omega) = \int_{-\infty}^{\infty} f(t)\, e^{-i\omega t}\, dt$$

$$= \int_{\tau_1}^{\tau_2} C_0 \sin\left(\omega_1 t + \theta\right) e^{-i\omega t}\, dt \,. \tag{A1}$$

By integrating and substituting limits,

$$F(\omega) = -\frac{C_0}{2}\left\{\frac{\cos\left[(\omega_1 - \omega)\tau_2 + \theta\right] - \cos\left[(\omega_1 - \omega)\tau_1 + \theta\right]}{\omega_1 - \omega}\right.$$

$$+ \frac{\cos\left[(\omega_1 + \omega)\tau_2 + \theta\right] - \cos\left[(\omega_1 + \omega)\tau_1 + \theta\right]}{\omega_1 + \omega}$$

$$+ i\,\frac{\sin\left[(\omega_1 - \omega)\tau_2 + \theta\right] - \sin\left[(\omega_1 - \omega)\tau_1 + \theta\right]}{\omega_1 - \omega}$$

$$\left. - i\,\frac{\sin\left[(\omega_1 + \omega)\tau_2 + \theta\right] - \sin\left[(\omega_1 + \omega)\tau_1 + \theta\right]}{\omega_1 + \omega}\right\} \tag{A2}$$

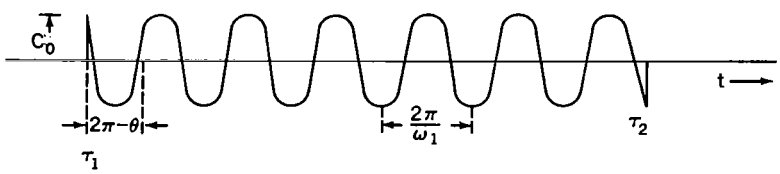

Figure A1—Pulsed sine wave.

This represents the general expression for the amplitude density spectrum of a pulsed sine wave of arbitrary phase and duration. The classic example is the case of a sine wave turned on at $-\tau/2$ and off at $+\tau/2$ with $\theta = 0$. The expression for this reduces to:

$$F(\omega) = \frac{C_0 \tau}{2} \left[\frac{\sin(\omega_1 - \omega)\frac{\tau}{2}}{(\omega_1 - \omega)\frac{\tau}{2}} - \frac{\sin(\omega_1 + \omega)\frac{\tau}{2}}{(\omega_1 + \omega)\frac{\tau}{2}} \right]. \tag{A3}$$

Appendix B

Autocorrelation Function for Gaussian Noise

With white additive Gaussian noise as the input to an ideal filter centered at ω_0 radians/sec and of bandwidth $\Delta\omega$ radians/sec, the autocorrelation of the output becomes:

$$\phi_{11}(\tau) = \frac{1}{2\pi}\int_{\omega_0 - \frac{\Delta\omega}{2}}^{\omega_0 + \frac{\Delta\omega}{2}} \frac{N}{2}\, e^{i\omega\tau}\, d\omega + \frac{1}{2\pi}\int_{-\left(\omega_0 + \frac{\Delta\omega}{2}\right)}^{-\left(\omega_0 - \frac{\Delta\omega}{2}\right)} \frac{N}{2}\, e^{i\omega\tau}\, d\omega \,, \tag{B1}$$

where N is the noise power density in watts per cps. Integrating and combining yields

$$\phi_{11}(\tau) = \frac{N}{2\pi}\left[\frac{\sin\left(\omega_0 + \frac{\Delta\omega}{2}\right)\tau}{\tau} - \frac{\sin\left(\omega_0 - \frac{\Delta\omega}{2}\right)\tau}{\tau}\right]. \tag{B2}$$

But

$$\sin(A + B) - \sin(A - B) = 2\cos A \sin B \,.$$

Therefore

$$\phi_{11}(\tau) = \frac{N\Delta\omega}{2\pi}\,\frac{\sin\Delta\omega\frac{\tau}{2}}{\Delta\omega\frac{\tau}{2}}\cos\omega_0\tau \,. \tag{B3}$$

Appendix C

Response of a Single-Pole Filter to a Step Sinusoid

The transfer function (Laplace transform) of the circuit in Figure 16 is:

$$\frac{E_0(s)}{E_{in}(s)} = \frac{\frac{1}{R}}{Cs + \frac{1}{R} + \frac{1}{Ls}}$$

$$= \frac{\frac{s}{RC}}{s^2 + \frac{1}{RC}s + \frac{1}{LC}} . \qquad \text{(C1)}$$

Substituting $\Delta\omega_0 = 1/RC$ and $\omega_0 = 1/\sqrt{LC}$ yields

$$\frac{E_0(s)}{E_{in}(s)} = \frac{\Delta\omega_0 s}{s^2 + \Delta\omega_0 s + \omega_0^2} . \qquad \text{(C2)}$$

This expression is in terms of the center frequency of the filter ω_0 and the bandwidth $\Delta\omega_0$. If the filter is excited with a step sinusoid $f(t) = A_1 \sin \omega_1 t \cdot u(t)$, where $u(t)$ is the unit step function, then

$$F(s) = \frac{A_1 \omega_1}{s^2 + \omega_1^2} . \qquad \text{(C3)}$$

Substituting gives

$$E_0(s) = \frac{\Delta\omega_0 s A_1 \omega_1}{(s^2 + \Delta\omega_0 s + \omega_0^2)(s^2 + \omega_1^2)} . \qquad \text{(C4)}$$

This is of the form

$$\frac{Ks}{(s^2 + as + b)(s^2 + c)} ,$$

where $a = \Delta\omega_0$, $b = \omega_0^2$, $c = \omega_1^2$, $K = \Delta\omega_0 \omega_1 A_1$.

By performing a partial fraction expansion and a few manipulations,

$$E_0(s) = \frac{\Delta\omega_0\,\omega_1\,A_1}{\left(\omega_1^2 - \omega_0^2\right) + \Delta\omega_0^2\,\omega_1^2}\left[\frac{\left(\omega_1^2 - \omega_0^2\right)s - \Delta\omega_0\,\omega_0^2}{s^2 + \Delta\omega_0 s + \omega_0^2} + \frac{\left(\omega_0^2 - \omega_1^2\right)s + \Delta\omega_0\,\omega_1^2}{s^2 + \omega_1^2}\right]. \qquad \text{(C5)}$$

Taking the inverse transform gives

$$e_0(t) = \frac{\Delta\omega_0\,\omega_1\,A_1}{\left(\omega_1^2 - \omega_0^2\right)^2 + \Delta\omega_0^2\,\omega_1^2}\left\{e^{-\Delta\omega_0 t/2}\left[\left(\omega_1^2 - \omega_0^2\right)^2 + \Delta\omega_0^2\left(\omega_1^2 + \omega_0^2\right)^2\right]^{1/2}\cdot\right.$$

$$\left.\cdot\sin\left(-\omega_0\sqrt{1 - \left(\frac{\Delta\omega_0}{2\omega_0}\right)^2}\;t + \phi_A\right) + \left[\left(\omega_0^2 - \omega_1^2\right)^2 + \Delta\omega_0^2\,\omega_1^2\right]^{1/2}\sin\left(\omega_1 t + \phi_B\right)\right\}, \qquad \text{(C6)}$$

where

$$\phi_A = \tan^{-1}\frac{\left(\omega_1^2 - \omega_0^2\right)2\omega_0\left[1 - \left(\frac{\Delta\omega_0}{2\omega_0}\right)^2\right]^{1/2}}{\Delta\omega_0\left(\omega_1^2 + \omega_0^2\right)},$$

$$\phi_B = \tan^{-1}\frac{\omega_0^2 - \omega_1^2}{\Delta\omega_0\,\omega_1}.$$

The response is now expressed as the sum of two sinusoids, one being the transient term and the other the steady state term. It is more advantageous to express the response as a single sinusoid. A modulating factor which is the envelope of the response will appear. Let $\omega_0 = \omega_1 + \Delta\omega_1$, where $\Delta\omega_1$ is the difference between the driven frequency and the resonant frequency. Making this substitution and neglecting second order terms yields

$$e_0(t) = \frac{\Delta\omega_0\,A_1}{\left(\Delta\omega_0^2 + 4\Delta\omega_1^2\right)^{1/2}}\left[-e^{-\Delta\omega_0 t/2}\sin\left(\omega_1 t + \Delta\omega_1 t - \phi_1\right) + \sin\left(\omega_1 t + \phi_2\right)\right], \qquad \text{(C7)}$$

where

$$\phi_1 = \tan^{-1}\left(-\frac{2\Delta\omega_1}{\Delta\omega_0}\right),$$

$$\phi_2 = \tan^{-1}\left(+\frac{2\Delta\omega_1}{\Delta\omega_0}\right).$$

Combining the two sinusoids yields

$$e_0(t) = \frac{\Delta\omega_0\,A_1}{\left(\Delta\omega_0^2 + 4\Delta\omega_1^2\right)^{1/2}}\left(1 + e^{-\Delta\omega_0 t} - 2e^{-\Delta\omega_0 t/2}\cos\Delta\omega_1 t\right)^{1/2}\sin\left(\omega_1 t + \phi_2 + \phi_3\right), \qquad \text{(C8)}$$

where

$$\phi_3 = \tan^{-1}\left(\frac{e^{-\Delta\omega_0 t/2}\sin\Delta\omega_1 t}{e^{-\Delta\omega_0 t/2}\cos\Delta\omega_1 t + 1}\right).$$

Appendix D

Response of a Single-Pole Filter to a Changing Frequency

From Appendix C the transfer function G(s) for the filter in Figure 16 is

$$G(s) = \frac{\Delta\omega_0 s}{s^2 + \Delta\omega_0 s + \omega_0^2} , \tag{D1}$$

where $\Delta\omega_0$ is the filter bandwidth and ω_0 is the filter center frequency. The response of the circuit to an impulse is

$$h(t) = L^{-1} \frac{\Delta\omega_0 s}{s^2 + \Delta\omega_0 s + \omega_0^2} \delta(t)$$

$$= \Delta\omega_0 e^{-\Delta\omega_0 t/2} \left[\cos \omega_0 \sqrt{1 - \left(\frac{\Delta\omega_0}{2\omega_0}\right)^2}\, t - \frac{\Delta\omega_0}{\omega_0 \sqrt{1 - \left(\frac{\Delta\omega_0}{2\omega_0}\right)^2}} \sin \omega_0 \sqrt{1 - \left(\frac{\Delta\omega_0}{2\omega_0}\right)^2}\, t \right] . \tag{D2}$$

For a reasonably high Q circuit

$$\sqrt{1 - \left(\frac{\Delta\omega_0}{2\omega_0}\right)^2} \approx 1$$

and

$$h(t) = \Delta\omega_0 e^{-\Delta\omega_0 t/2} \left(\cos \omega_0 t - \frac{\Delta\omega_0}{2} \sin \omega_0 t \right) \tag{D3}$$

$$= \Delta\omega_0 e^{-\Delta\omega_0 t/2} \left(1 + \frac{\Delta\omega_0}{2\omega_0} \right)^{1/2} \cos \left(\omega_0 t + \tan^{-1} \frac{\Delta\omega_0}{2\omega_0} \right)$$

$$\approx \Delta\omega_0 e^{-\Delta\omega_0 t/2} \cos \left(\omega_0 t + \tan^{-1} \frac{\Delta\omega_0}{2\omega_0} \right) . \tag{D4}$$

The driving function for the filter is a step sinusoid with varying frequency. The rate of change of phase is given by

$$\frac{d\phi(t)}{dt} = \omega_1 + \omega_d \sin \omega_a t , \tag{D5}$$

where ω_1 is the center frequency of driving function, ω_d is the peak frequency deviation, and ω_a is the modulation frequency. Integration yields

$$\phi(t) = \omega_1 t - \frac{\omega_d}{\omega_a} \cos \omega_a t + C_1 \quad . \tag{D6}$$

With this expression for the phase of the driving function and $C_1 = 0$,

$$f(t) = A_1 \sin\left(\omega_1 t - \frac{\omega_d}{\omega_a} \cos \omega_a t\right) \cdot u(t) \quad . \tag{D7}$$

The response can be expressed as the convolution of the driving function with the response of the system to an impulse:

$$h(t) = \int_0^t f(\tau)\, g(t - \tau)\, d\tau \quad . \tag{D8}$$

And, by substitution,

$$h(t) = \int_0^t A_1 \sin\left(\omega_1 \tau - \frac{\omega_d}{\omega_a} \cos \omega_a \tau\right) \cdot \Delta\omega_0 e^{-\Delta\omega_0 (t-\tau)/2} \cos\left[\omega_0 (t - \tau) + \tan^{-1} \frac{\Delta\omega_0}{2\omega_0}\right] d\tau$$

$$= \Delta\omega_0 A_1 e^{-\Delta\omega_0 t/2} \left[\cos\left(\omega_0 t + \tan^{-1} \frac{\Delta\omega_0}{2\omega_0}\right) \int_0^t e^{\Delta\omega_0 \tau/2} \cos \omega_0 \tau \cdot \sin\left(\omega_1 \tau - \frac{\omega_d}{\omega_a} \cos \omega_a \tau\right) d\tau \right.$$

$$\left. + \sin\left(\omega_0 t + \tan^{-1} \frac{\Delta\omega_0}{2\omega_0}\right) \int_0^t e^{\Delta\omega_0 \tau/2} \sin \omega_0 \tau \cdot \sin\left(\omega_1 \tau - \frac{\omega_d}{\omega_a} \cos \omega_a \tau\right) d\tau \right] \quad . \tag{D9}$$